Novel functions of the ubiquitin-independent proteasome system in regulating *Xenopus* germline development

Hyojeong Hwang[1], Zhigang Jin[1, 2], Vishnu Vardhan Krishnamurthy[3], Anumita Saha[4], Peter S. Klein[5], Benjamin Garcia[4], Wenyan Mei[1], Mary Lou King[6], Kai Zhang[3], and Jing Yang[1, §]

[1]Department of Comparative Biosciences, University of Illinois at Urbana-Champaign, 2001 South Lincoln Avenue, 3411 Veterinary Medicine Basic Sciences Building, Urbana, IL 61802, USA

[2]College of Chemistry and Life Sciences, Zhejiang Normal University, 688 Yingbin Road, Jinhua, Zhejiang 321004, China

[3]Department of Biochemistry, University of Illinois at Urbana-Champaign, 600 S Mathews, 314B Roger Adams Laboratory, Urbana, IL 61801, USA.

[4]Epigenetics Institute, Department of Biochemistry and Biophysics, Perelman School of Medicine at the University of Pennsylvania, 3400 Civic Center Blvd, Philadelphia, PA 19104, USA.

[5]Department of Medicine (Hematology-Oncology), Perelman School of Medicine at the University of Pennsylvania, Philadelphia, PA, 19104, USA.

[6]Department of Cell Biology, University of Miami Miller School of Medicine, 1011 NW 15th St, Miami, FL 33136, USA.

[§]***To whom correspondence should be addressed***

***Key words*:** Ubiquitin-independent proteasome, Dnd1, germline development, oocyte-to-embryo transition, *Xenopus*

Summary Statement

We investigate the mechanisms by which Dnd1 protein is regulated during the oocyte-to-embryo transition. Our results uncover novel regulation and inhibitory functions of the ubiquitin-independent proteasome during vertebrate germline development.

Abstract

In most species, early germline development occurs in the absence of transcription with germline determinants subject to complex translational and post-translational regulations. Here we report for the first time, that early germline development is influenced by dynamic regulation of the proteasome system, previously thought to be ubiquitously expressed and to serve "house-keeping" roles in controlling protein homeostasis. We show that proteasomes are present in a gradient with highest levels in the animal hemisphere but extending into the vegetal hemisphere of *Xenopus* oocytes. This distribution changes dramatically during the oocyte-to-embryo transition, with proteasomes becoming enriched in and restricted to the animal hemisphere and therefore separated from vegetally localized germline determinants. We identify Dead-end1 (Dnd1), a master regulator of vertebrate germline development, as a novel substrate of the ubiquitin-independent proteasomes. In the oocyte, ubiquitin-independent proteasomal degradation acts together with translational repression to prevent premature accumulation of Dnd1 protein. In the embryo, artificially increasing ubiquitin-independent proteasomal degradation in the vegetal pole interferes with germline development. Our work thus reveals novel inhibitory functions and spatial regulation of the ubiquitin-independent proteasome during vertebrate germline development.

Introduction

The primordial germ cells (PGCs), which give rise to sperm and oocytes in adult animals, are considered the "stem cells of the species" (Wylie, 1999, Seydoux and Braun, 2006). Specification of PGCs occurs through different mechanisms in different species. In mammals, PGCs are induced after implantation when proximal cells in the epiblast receive BMP signals from extra-embryonic tissues. In contrast, *Drosophila*, *C. elegans*, zebrafish, and *Xenopus* specify their PGCs through inheritance of germ plasm (Aguero et al., 2017b, Extavour and Akam, 2003, Saitou, 2009, Strome and Lehmann, 2007, Tam and Zhou, 1996, Lawson et al., 1999, Ying et al., 2001, Ohinata et al., 2009). Despite the differences in how PGCs are specified, ~80% of transcripts enriched in amphibian PGCs (Butler et al., 2018) are expressed in human gonadal PGCs (Irie et al., 2015). Many aspects of PGC development are highly conserved across species. In animals such as *Drosophila*, *C. elegans*, zebrafish, and *Xenopus*, the genetic program responsible for early PGC development is encoded by maternally expressed germ plasm RNAs and proteins. After fertilization, these factors act in a precisely regulated fashion to direct the specification, proliferation, and migration of PGCs. How early germline development is orchestrated by translational and post-translational regulatory mechanisms remains unclear.

In animals that specify the germline through inheritance of the germ plasm, RNAs coding for germline determinants are transcribed during early oogenesis and asymmetrically localized in the oocyte. Translation of many germline specific RNAs is dynamically regulated. This is particularly true for germline determinants that promote PGC development by suppressing somatic differentiation. These proteins are often expressed at very low levels, or not at all, in fully-grown oocytes. Accumulation of these factors occurs after fertilization when germline development is initiated (Yang et al., 2015). Premature expression of these germline

determinants in the oocyte may result in ectopic distribution of these factors, which later interferes with the development of somatic tissues in the embryo (Luo et al., 2011, Mei et al., 2013).

One such factor is Dnd1, an evolutionarily conserved RNA binding protein essential for vertebrate germline development (Gross-Thebing et al., 2017, Weidinger et al., 2003, Youngren et al., 2005, Horvay et al., 2006, Cook et al., 2009). During early embryonic development, Dnd1 prevents somatic differentiation of PGCs (Gross-Thebing et al., 2017), at least partially through promoting the expression of Nanos1 (Kedde et al., 2007, Aguero et al., 2017a, Aguero et al., 2018), which represses translation of somatic genes in PGCs (Nakahata et al., 2001, Sonoda and Wharton, 1999, Sonoda and Wharton, 2001, Jaruzelska et al., 2003, Schaner et al., 2003, Deshpande et al., 1999, Sato et al., 2007, Lai et al., 2012). In *Xenopus*, Dnd1 protein is highly expressed during cleavage and blastula stages to promote *nanos1* translation (Aguero et al., 2017a). Interestingly, a very low level of Dnd1 protein expressed in the vegetal cortex in the oocyte (Aguero et al., 2017a) maintains vegetal localization Trim36 protein by anchoring *trim36* mRNA to the vegetal cortex (Mei et al., 2013). After fertilization, vegetally localized Trim36 promotes microtubule assembly during cortical rotation and subsequent dorsal development (Cuykendall and Houston, 2009). The level of Dnd1 protein must be tightly controlled in the oocyte. Knockdown of Dnd1 in the oocyte disrupts asymmetric localization of *trim36* and results in ventralized embryos (Mei et al., 2013). On the other hand, overexpression of Dnd1 triggers premature *nanos1* translation in the oocyte (Aguero et al., 2017a), impairing early embryonic patterning (Mei et al., 2013). Currently it is unclear how the expression of Dnd1 protein is precisely regulated.

The temporal and spatial expression of proteins is often orchestrated by dynamically regulated transcription, translation, and protein turnover. By promoting protein turnover, the proteasome system, together with the autophagy/lysosome system, plays a major role in controlling the expression of proteins (Wong and Cuervo, 2010). The proteasome system consists of several types of macromolecular complexes capable of proteolysis inside the cell. The proteolytic activity of the proteasome resides in the 20S proteasome core particle (20S CP), a complex of 28 subunits. Protein substrates are recruited to the 20S CP by several types of proteasome activators. These include 19S regulatory particle (19S RP), proteasome activators PSME1 (PA28α), PSME2 (PA28β), PSME3 (PA28γ), and PSME4 (PA200). Among these, 19S RP, which forms the 26S proteasome together with 20S CP, recruits polyubiquitinated proteins in an ATP-dependent manner. PSME1, PSME2, PSME3, and PSME4 are responsible for recruiting non-ubiquitinated protein substrates. PSME1/PSME2 and PSME3 form hetero- or homo-heptameric complexes, respectively. PSME4 acts as a monomer to open the gate of the 20S CP (Hwang et al., 2011, Rechsteiner and Hill, 2005, Kish-Trier and Hill, 2013, Ben-Nissan and Sharon, 2014). Involvement of ubiquitin-independent proteasome during germline development has been previously documented (Khor et al., 2006, Qian et al., 2013, Huang et al., 2016). In mice, compound mutants for PSME3 and PSME4 are completely infertile in males (Huang et al., 2016). So far, only acetylated core histones have been identified as substrates of ubiquitin-independent proteasomes during germline development (Qian et al., 2013). Additional substrates and roles of the ubiquitin-independent proteasome in germline development remain uncharacterized.

Here we report that two inhibitory mechanisms, *dnd1* translational repression and ubiquitin-independent proteasomal turnover of Dnd1, act together to prevent premature accumulation of Dnd1 protein before fertilization. These inhibitory mechanisms are relieved during the oocyte-to-embryo transition, allowing an abrupt increase in the level of Dnd1 protein. Our results further reveal that the proteasome system undergoes a dramatic relocalization during the oocyte-to-embryo transition. Consequently, proteasomes become separated from vegetally localized *dnd1* and other germ plasm components in the embryo. Ectopic expression of PSME1/PSME2, PSME3, and PSME4 in the vegetal pole of the embryo impairs PGC development. Our study thus uncovers novel functions of the ubiquitin-independent proteasome in regulating vertebrate germline development.

Results

Translation of *dnd1* is repressed in the oocyte of *Xenopus laevis*

We previously reported that a low level of Dnd1 protein is expressed in the oocyte (Aguero et al., 2017a), where it anchors *trim36* RNA to the vegetal cortex (Mei et al., 2013). After fertilization, the expression of Dnd1 increases abruptly to promote *nanos1* translation, essential for germline development (Aguero et al., 2017a). Consistent with these observations, we found that the expression level of Dnd1 protein was low in the oocyte and egg, but increased significantly after fertilization (Fig 1A). Interestingly, after germinal vesicle breakdown (GVBD), nearly 50% of Dnd1 protein is phosphorylated (Supplemental Fig 1). To understand how the expression of Dnd1 protein is controlled, we first investigated *dnd1* translational regulation. We focused on the 3'UTR of *dnd1*, because *dnd1* contains a very short 5'UTR, and unlikely to be important for translational regulation. We generated a GFP-myc-dnd3'UTR by

fusing the 3'UTR of *Xenopus tropicalis dnd1* to a myc-tagged GFP. GFP-myc-SV40, in which myc-GFP was fused with a SV40 polyA signal, was used as the well-translated control. RNAs (250 pg) coding for GFP-myc-dnd3'UTR and GFP-myc-SV40 were injected into fully-grown oocytes. Injected oocytes were cultured for 24 hours, treated with progesterone to induce oocyte maturation, and artificially activated by pricking with a glass needle. The expression of myc-GFP was monitored by western blot. As shown in Figure 1B, the expression level of GFP-myc-dnd3'UTR was lower than that of GFP-myc-SV40 in fully-grown oocytes, suggesting that *dnd1* translation is repressed in the fully-grown oocyte. After GVBD, we detected a dramatic increase in the expression of GFP-myc-dnd3'UTR. After egg activation, the expression level of GFP-myc-dnd3'UTR further increased by 2-3-fold over the four-hour period (Fig 1B). To test directly if the 3'UTR of *dnd1* contains cis-regulatory element(s) that represses its translation in the oocyte, we inserted the complete 3'UTR of *dnd1* into GFP-myc-SV40 (nucleotide 1130-1735, Fig 1C). In the oocyte, the expression level of 1130-1735 was lower than that of GFP-myc-SV40. After GVBD, while the expression GFP-myc-SV40 remained unchanged, the expression of 1130-1735 increased. Using the same strategy, we tested the 3'UTR of *Xenopus laevis dnd1* and found it behaved essentially the same as the 3'UTR of *tropicalis dnd1* (Fig 1D). Based on these results, we conclude that the 3'UTR of *dnd1* contains cis-regulatory element(s) that represses *dnd1* translation in the oocyte. This repression is relieved after GVBD.

Dnd1 protein is intrinsically unstable

While translational repression of *dnd1* is relieved after oocyte maturation, the expression of endogenous Dnd1 protein remains at a low level in the egg. This observation suggests that protein turnover plays an important role in preventing premature accumulation of Dnd1 protein before fertilization. To assess Dnd1 protein turnover in the oocyte, we depleted *dnd1* mRNA by injection of the *dnd1* antisense oligo (As-oligo) (Mei et al., 2013), and monitored the levels of endogenous *dnd1* mRNA and Dnd1 protein. We found that at 2 hours post As-oligo injection, Dnd1 protein was reduced below 50% (Fig 2A and B), demonstrating that Dnd1 protein has a short half-life in the oocyte. In parallel to this experiment, we fused Dnd1 to GFP and compared the expression of GFP and GFP-Dnd1 in the oocyte and embryo. In the oocyte, although GFP was clearly expressed, we could barely detect GFP-Dnd1. By contrast, GFP and GFP-Dnd1 were expressed at comparable levels in the embryo (Fig 2C). This result confirms that Dnd1 is unstable in the oocyte. To assess the half-life of Dnd1 protein directly, we blocked protein synthesis by treating oocytes and embryos with cycloheximide (CHX) and measured the level of endogenous Dnd1 protein at multiple time points. We found that the half-life of Dnd1 in the oocyte is ~70 minutes. In the embryo, however, the half-life of Dnd1 protein is close to 4 hours. In HEK293T cells, the half-life of overexpressed Dnd1-myc is ~2 hours (Fig 2D). Taken together, we conclude that Dnd1 is intrinsically unstable in the oocyte, but becomes stable after fertilization.

Identification of the degron that promotes Dnd1 turnover in the oocyte of *Xenopus laevis*

To identify the degron that targets Dnd1 protein for rapid degradation in the oocyte, we fused various deletions of Dnd1 to GFP-myc (Fig 3A). RNAs coding for GFP-myc and fusion proteins (200 pg each) were injected into oocytes, followed by western blot analysis (Fig 3B). Compared to GFP, all fusion proteins carrying an evolutionarily conserved motif located between residue 107 and 127 of Dnd1 (Fig 3C) were poorly expressed in the oocyte. In contrast, all constructs lacking this motif were expressed at comparable levels as that of GFP-myc (Fig 3A and B). To determine if this degron functions specifically in the oocyte, we transfected $GFP_{D107\text{-}127}$ into HEK293T cells. While GFP-myc was abundantly expressed, we could detect only a trace amount of $GFP_{D107\text{-}127}$ protein (Fig 3D). RT-qPCR revealed that transcription of $GFP_{D107\text{-}127}$ and GFP-myc was comparable (Fig 3E). In parallel, we fused various copies of D107-127 to luciferase and expressed them in NIH3T3 cells. The luciferase assay revealed that D107-127 decreased the expression of luciferase in a dose-dependent manner (Fig 3F). Thus, D107-127 is a potent degron capable of promoting protein degradation not only in the oocyte, but also in mammalian somatic cells. We generated a truncated Dnd1 lacking this degron ($\Delta_{D107\text{-}119}$). As expected, $\Delta_{D107\text{-}119}$ is much more stable than the wild type Dnd1-myc in the oocyte and in HEK239T cells (Fig 3G). Collectively, these results demonstrate that D107-127 targets Dnd1 for rapid degradation in the oocyte.

By blasting the *Xenopus* protein database using the sequence of D107-127, we found a few proteins with a similar motif. These include hnRNP R, Syncrip, A1CF, RBM47, and RBM46 (Fig 4A). We generated myc-tagged constructs and transfected them into HEK293T cells. While Dnd1 and RBM46 were poorly expressed, hnRNP R, Syncrip, and A1CF were expressed at much higher levels (Fig. 4B). Since Phenylalanine 110 in Dnd1 is uniquely conserved between Dnd1 and RBM46, and not in the other proteins, we generated a F110M mutant to test the significance of F110. As a control, we also mutated S117, a residue that is not uniquely conserved in Dnd1 and RBM46, by replacing the Serine residue with an Aspartic acid residue (S117D). When overexpressed in the oocyte, the expression of F110M was much higher than that of the wild type Dnd1. In the embryo, F110M and the wild type Dnd1 were expressed at a comparable level (Fig 4C). These results indicate that residue F110 is essential for D107-127 to function as a degron, and further support our conclusion that the stability of Dnd1 is differentially regulated before and after fertilization. To determine if overexpression of F110M would affect germline line development, we injected RNA encoding F110M into the vegetal pole of fertilized eggs. We found overexpression of F110M had little effect on the number of PGCs at the tailbud stage (Supplemental Fig 2).

D107-127 promotes ubiquitin-independent proteasome turnover

To better understand Dnd1 turnover, we transfected myc-Dnd1 and myc-GFP into HEK293T and GC-2spd cells, an immortalized mouse spermatocyte cell line (Hofmann et al., 1994). Transfected cells were treated with various inhibitors that selectively inhibit proteasome, lysosome, or autophagy. In both HEK293T and GC-2spd cells, the proteasome inhibitor MG132 significantly increased the expression of myc-Dnd1 protein (Fig 5A). Lactacystin, another

proteasome inhibitor, increased the expression of Dnd1 too, albeit to a lesser extent, likely because of the difference in the potency of the two inhibitors. Both MG132 and Lactacystin induced a high molecular weight smear of myc-Dnd1, indicative of polyubiquitination of Dnd1 protein. The autophagy inhibitor 3MA increased the expression of Dnd1 in HEK293T cells, but failed to do so in GC-2spd cells, suggesting that Dnd1 may be regulated by autophagy in a context-dependent manner. Ammonium chloride, which inhibits lysosomal degradation by neutralizing the low pH of lysosome, had no detectable effect on Dnd1 in both cell lines. Since we were interested in Dnd1 turnover in oocytes, we chose to focus on the proteasome.

To determine if D107-127 targets Dnd1 to the ubiquitin proteasome pathway, we transfected myc-Dnd1, $\Delta_{D107-119}$, and $GFP_{D107-127}$ into GC-2spd cells. We found that MG132 treatment increased the expression of myc-Dnd1, $\Delta_{D107-119}$, and $GFP_{D107-127}$. Surprisingly, we observed MG132-induced high molecular weight smear of myc-Dnd1 and $\Delta_{D107-119}$, but not for $GFP_{D107-127}$ (Fig 5B). This raises the striking possibility that while Dnd1 can be degraded by the ubiquitin/proteasome system, D107-127 targets Dnd1 to the proteasome degradation pathway in a ubiquitin-independent manner. To strengthen this conclusion, we overexpressed myc-Dnd1, $\Delta_{D107-119}$, and $GFP_{D107-127}$ together with HA-tagged Ubiquitin (HA-Ub) and cultured cells in the presence of MG132. Myc-Dnd1, $\Delta_{D107-119}$, and $GFP_{D107-127}$ were immunoprecipitated using an anti-myc antibody and probed for HA-Ubiquitin. Indeed, the high molecular weight smear of myc-Dnd1 and $\Delta_{D107-119}$ was recognized by the HA antibody, demonstrating that myc-Dnd1 and $\Delta_{D107-119}$ were polyubiquitinated (Fig 5C). By contrast, $GFP_{D107-127}$ was not recognized by the HA antibody (Fig 5C), arguing strongly that D107-127 targets Dnd1 to the ubiquitin-independent proteasome pathway.

Inside the cell, non-ubiquitinated proteins are recruited to the proteasome by the PSME1/2 heteroheptamer, PSME3 homoheptamer, or PSME4 monomer (Hwang et al., 2011, Rechsteiner and Hill, 2005, Kish-Trier and Hill, 2013, Ben-Nissan and Sharon, 2014). To determine if PSME1/2, PSME3, or PSME4 are required for D107-127-mediated proteasome turnover of Dnd1, we generated dominant negative (dn) proteasome activators. Our results reveal that overexpression of dnPSME1 (PSME1 N141Y), dnPSME2 (PSME2 N139Y), dnPSME3 (PSME3 N151Y) (Zhang et al., 1998), or dnPSME4 (PSME4$^{1635\text{-}1723}$, the BRDL region of PSME4) (Qian et al., 2013) individually did not stabilize $GFP_{D107\text{-}127}$. By contrast, $GFP_{D107\text{-}127}$ was stabilized when all four dominant negative constructs were co-overexpressed (Fig 5D). Consistently, co-overexpression of all four dominant negative proteasome activators increased the level of endogenous Dnd1 protein in the oocyte (Fig 5E and F). This suggests that PSME1/2, PSME3, and PSME4 function redundantly to promote ubiquitin-independent Dnd1 turnover in the oocyte.

Mutation of degron D107-127 increases the expression of Dnd1 in the oocyte, but fails to do so in the embryo (Fig 3G and 4C). This indicates that the ubiquitin-independent proteasomal turnover of Dnd1 is inhibited after fertilization. In principle, this may be caused by inhibition of the ubiquitin-independent proteasome pathway after fertilization. Alternatively, a regulatory mechanism may be activated after fertilization to protect Dnd1 from ubiquitin-independent proteasomal degradation in the embryo. To distinguish between these possibilities, we assessed the expression of several Dnd1 GFP fusion constructs in the embryo. All of these constructs contain degron D107-127, which is located in RRM1, but vary in their N- or C-terminal sequences (Fig 5G). Our results revealed that $GFP_{D96\text{-}247}$, $GFP_{D96\text{-}C}$, $GFP_{D1\text{-}127}$, and $GFP_{D96\text{-}127}$

were poorly expressed in the embryo. In contrast, the expression of GFP_{D1-247}, $GFP_{D72-151}$, and GFP-Dnd1 was similar to that of myc-GFP (Fig 5H). It appears that all Dnd1 deletion constructs lacking an intact RRM1 are unstable in the embryo, whereas constructs containing an intact RRM1 are stable (Fig 5G). These results demonstrate that the ubiquitin-independent proteasome pathway is active in the embryo, and argue for the existence of a regulatory mechanism that acts on the RRM1 to prevent Dnd1 from ubiquitin-independent proteasomal degradation after fertilization.

Dynamic expression of the proteasome system during the oocyte-to-embryo transition

Inspired by the above findings, we examined the expression of *psme1*, *psme2*, *psme3*, and *psme4*. RT-PCR results reveal that total levels of *psme1*, *psme2*, *psme3*, and *psme4* RNAs remain unaltered during the oocyte-to-embryo transition (Fig 6A). In stark contrast, the subcellular localization of these RNAs changes dramatically during the oocyte-to-embryo transition. In the oocyte, *psme1*, *psme2*, *psme3*, and *psme4* RNAs form a smooth gradient along the animal-vegetal axis, with the highest concentration of RNAs being detected in the animal pole. In the vegetal hemisphere, the trailing end of *psme1*, *psme2*, *psme3*, and *psme4* overlaps with *pgat* (Hudson and Woodland, 1998) and *dnd1* (Horvay et al., 2006), germ plasm RNAs that are transported to the vegetal pole during oogenesis through the early and late localization pathways, respectively (Kloc et al., 2001, Kloc and Etkin, 2005). In the mature egg, *psme1*, *psme2*, *psme3*, and *psme4* RNAs become restricted to the animal hemisphere, with a boundary at the equator that separates them from vegetally localized *pgat* and *dnd1*. This pattern persists after fertilization. At the 2-cell stage, RNAs coding for proteasome activators remain restricted to the animal hemisphere (Fig 6B).

We extended our analysis by examining the expression of *psmc6* and *psma2*, which encode components of the 19S regulatory particle (RP) and 20 core particle (CP), respectively. In situ hybridization results revealed that the expression pattern of *psmc6* and *psma2* was essentially the same as that of *psme1*, *psme2*, *psme3*, and *psme4*, forming a gradient along the animal-vegetal axis in the oocyte, but becoming uniformly distributed in the animal hemisphere after maturation (Fig 6B). We also examined the expression of *eIF4A1* and *eIF4E*, two house-keeping genes that encode key components of the translational machinery. *eIF4A1* and *eIF4E* can be detected in the entire oocyte, but are more abundant in the animal hemisphere. This pattern remains unchanged during the oocyte-to-embryo transition (Fig 6B).

We further examined the subcellular distribution of 20S CP during the oocyte-to-embryo transition by immunofluorescence. Similar to the dynamic expression pattern of RNAs coding for proteasome components, we found that 20S CP formed an animal to vegetal gradient in the oocyte. After oocyte maturation, the staining signal became stronger in the animal hemisphere. In 2-cell stage embryo, the animal/vegetal difference is more obvious, most likely due to newly synthesis of proteasome components in the animal hemisphere (Fig 6C). It appears that the proteasome system undergoes a dramatic vegetal-to-animal relocalization during the oocyte-to-embryo transition. To further confirm the graded distribution of the proteasome system in early embryos, cytoplasm was collected from animal and vegetal hemispheres of 1-cell stage embryos using a micropipette based nanofluidic device (Saha-Shah et al., 2015). The harvested cytoplasm was analyzed directly by shotgun proteomics (Saha-Shah et al. manuscript under review). We detected several proteasome components, including PSMA2, PSMA3, PSMA4, PSMA5, PSMA6, PSMB1, PSMB3, PSMB4, PSME1, and PSME3 (Supplemental Table 1). Consistent

with immunofluorescence of 20S CP, we found all PSMAs, PSMBs and PSME1 were enriched in the animal hemisphere. Compared to the above proteasome components, PSME3 was detected at low levels by mass spectrometry (Fig 6D) and hence quantified with lesser confidence. We believe that the lower apparent enrichment of PSME3 in the animal hemisphere relative to other components of 20S CP is due to the difficulty in detecting this low abundance protein. Collectively, our immunofluorescence and proteomic data support the conclusion that proteasomes are enriched in the animal hemisphere in early *Xenopus* embryos.

The above results raise the striking possibility that the vegetal-to-animal relocalization of the proteasome system may be a prerequisite for the germline development in the embryo. We thus determined if overexpression of wild-type PSME, PSME2, PSME3, and PSME4, which prevent premature expression Dnd1 in the oocyte, would interfere with PGC development. We injected *psme1+psme2* (1 ng each), *psme3* (1 ng), *psme4* (1 ng), or a combination of all four mRNAs (330 pg each) into the vegetal pole of 1-cell stage embryos. These embryos were harvested at the late tailbud stage and analyzed by *in situ* hybridization for *pgat*, a widely used marker for PGCs (Hudson and Woodland, 1998). We found that the number of *pgat*-positive PGCs were significantly reduced in PSME1+PSME2, PSME3, and PSME4 overexpressed embryos (Fig 7A and B). Some of PSME4 overexpressed embryos were cultured until stage 48. Importantly, we did not detect any morphological or histological abnormalities in PSME4 overexpressed embryos (Supplemental Fig 4). It appears that overexpression of ubiquitin-independent proteasome activators in the vegetal pole specifically affects germline development. We conclude that the vegetal-to-animal translocation of *psme1*, *psme2*, *psme3*, and *psme4* during the oocyte-to-embryo transition is critically important for PGC development after fertilization.

Since Dnd1 is protected from the ubiquitin-independent proteasome after fertilization (Fig 5G and H), we speculated that the ubiquitin-independent proteasome is capable of degrading other PGC regulators in the embryo. We tested three germ plasm components that are abundantly expressed in PGCs (Butler et al., 2018), including Trim36 (Cuykendall and Houston, 2009), Dazl (Houston and King, 2000, Houston et al., 1998), and Nanos1 (Zhou and King, 1996, Lai et al., 2012, Lai et al., 2011, Luo et al., 2011). At the 1-cell stage, RNAs encoding myc-Trim36 (100 pg), myc-Dazl (100 pg), and myc-Nanos1 (100 pg) were injected into the vegetal pole along, or together with wild type *psme4* (1 ng). At stage 9, embryos were harvested for western blot analysis. As shown in Figure 7C, overexpression of PSME4 reduced the expression of Trim36, without affecting Dazl and Nanos1. This suggests that the ubiquitin-independent proteasome interferes with PGC development by promoting degradation of a subset of germ plasm components.

Discussion

During early embryogenesis, Dnd1 regulates PGC development (Weidinger et al., 2003, Horvay et al., 2006, Gross-Thebing et al., 2017) by protecting germline specific RNAs and promoting the expression of PGC regulators (Kedde et al., 2007, Koebernick et al., 2010, Aguero et al., 2017a). In *Xenopus*, a low level of Dnd1 protein is expressed in the oocyte (Aguero et al., 2017a) and plays a pivotal role in anchoring *trim36* to the vegetal cortex (Mei et al., 2013). After fertilization, vegetally localized Trim36 regulates polymerization of microtubules during cortical rotation, allowing transportation of dorsal determinants to the future dorsal side of the embryo (Cuykendall and Houston, 2009). While knockdown of Dnd1 in the oocyte disrupts microtubule assembly during cortical rotation and results in ventralized embryos, overexpression of Dnd1 in

the oocyte impairs early embryonic development as well (Mei et al., 2013), presumably by triggering premature *nanos1* translation in oocytes (Aguero et al., 2017a), which interferes with the development of soma (Luo et al., 2011). The goal of the current study was to understand how Dnd1 protein is so precisely regulated at the translational- and post-translational levels.

The results presented here reveal two mechanisms that act together to prevent premature accumulation of Dnd1 protein before fertilization. These include translational repression, mediated by the inhibitory element(s) in the 3'UTR of *dnd1* RNA, and ubiquitin-independent proteasome degradation of Dnd1 protein. Translational repression of *dnd1* is relieved after GVBD. Dnd1 protein is protected from the ubiquitin-independent proteasome pathway in the embryo, possibly due to post-translational modification of RRM1 or the expression of a RRM1-binding protein after fertilization which reduces the proteasomal accessibility of Dnd1. As a consequence of inactivation of these inhibitory mechanisms during the oocyte-to-embryo transition, Dnd1 protein accumulates in the embryo. Interestingly, we found Dnd1 can be regulated by the ubiquitin-dependent proteasome and autophagy in vitro. It is possible that these protein turnover mechanisms each contribute to overall regulation of Dnd1 protein during early germline development.

The finding that Dnd1 is degraded by the ubiquitin-independent proteasome pathway is intriguing. While functions of the 26S proteasome, which degrades polyubiquitinated substrates, have been documented by a large body of literature (for review, see (Muller and Schwartz, 1995, DeRenzo and Seydoux, 2004, Bowerman and Kurz, 2006, Karabinova et al., 2011, Tsukamoto and Tatsumi, 2018)), little is known about the ubiquitin-independent proteasome during

development. Only a handful of substrates for the ubiquitin-independent proteasome have been identified (Hoyt and Coffino, 2004). Some recent studies uncovered roles of ubiquitin-independent proteasome during spermatogenesis (Huang et al., 2016, Qian et al., 2013) and identified acetylated core histones as substrates for the ubiquitin-independent proteasome (Qian et al., 2013). However, roles of the ubiquitin-independent proteasome during germline development are largely unknown. Our results demonstrate that in *Xenopus*, Dnd1 and Trim36 are novel substrates for the ubiquitin-independent proteasome. In the case of Dnd1, degron D107-127, a small motif located in the RRM1, targets Dnd1 to the ubiquitin-independent proteasome pathway. Mutation of this degron leads to stabilization of Dnd1 protein in the oocyte. The sequence of D107-127 is similar to a motif found in TRP2 (amino acid residues 181-193), which is processed by PSME1/PSME2-containing proteasome (Murata et al., 2001). Consistent with our observation, Li et al. recently identified several mutations that promote proteasomal degradation of Dnd1. These mutations are located in the RRM1 of Dnd1 and alters the structure around degron D107-127 (Li et al., 2018). We show protein degradation mediated by degron D107-127 could be blocked in *Xenopus* oocytes when dnPSME1, dnPSME2, dnPSME3, and dnPSME4 were co-expressed. This demonstrates that PSME1/PSME2, PSME3, and PSME4-containing proteasomes function redundantly to prevent accumulation of Dnd1 protein in the oocyte, highlighting a novel function of the ubiquitin-independent proteasome in preventing premature initiation of germline development.

Our work reveals that *psme1*, *psme2*, *psme3*, and *psme4*, and other proteasome RNAs (*psme6* and *psma2*) form an animal-to-vegetal gradient in the oocyte. The distribution of these RNAs changes dramatically during the oocyte-to-embryo transition. By 2-cell stage, these RNAs are restricted to the animal hemisphere and become separated from vegetally localized germ plasm. This observation is consistent with results from a recently published RNAseq analysis (Sindelka et al., 2018). We assessed the subcellular localization of 20S CP by immunofluorescence and observed similar dynamic changes, albeit with a slower kinetic. Although 20S CP is only slightly enriched in the animal hemisphere in the oocyte and egg, we detected a much larger animal/vegetal difference by the 2-cell stage, likely due to new synthesis of proteasome in the animal hemisphere. We collected cytoplasm from animal and vegetal hemispheres of fertilized eggs and performed proteomic analysis. Quantitative proteomic measurement confirms that proteasome components are animally enriched at the 1-cell stage. Our results further indicate that overexpression of ubiquitin-independent proteasome activators in the vegetal pole of embryos reduced the expression of Trim36 during blastula stages and decreased the number of PGCs at the tailbud stage. These observations support our model that relocalization of ubiquitin-independent proteasomes during the oocyte-to-embryo transition reduces proteasomal turnover rate in the vegetal pole, creating a permissive environment for germline development after fertilization (Fig 7D).

We have noticed that the graded distribution of the proteasome was not detected in a recently published proteomic study (Sindelka et al., 2018). This discrepancy is likely caused by the difference in sampling methods to harvest cytoplasmic proteins. In our study, we used two orthogonal approaches to assess the subcellular localization of 20S CP. First, we demonstrated animal hemisphere enrichment by immunofluorescence. Second, we collected cytoplasm from animal and vegetal hemispheres of otherwise unperturbed fertilized eggs using a micropipette and cytoplasm was then analyzed directly by mass spectrometry. In contrast, Sindelka et al., extracted proteins from relatively large pieces of eggs using a bottom-up proteomic sample preparation approach coupling NP40 extraction with filter (Sindelka et al., 2018). While this method effectively reduces contamination from yolk proteins, other proteins, including proteasomal proteins, may also have been removed during sample preparation.

It is worth mentioning that germline specific RNAs *dnd1* and *pgat* remain vegetally localized during the oocyte-to-embryo transition. The distribution of *eIF4A1* and *eIF4E*, which encode proteins essential for translation, is not changed at all. Thus, not all maternal RNAs undergo vegetal-to-animal translocation during the oocyte-to-embryo transition. Nevertheless, it seems unlikely that this reorganization event is specific to proteasome RNAs. The vegetal-to-animal translocation of proteasome is reminiscent of the massive rearrangement of yolk platelets and deep cytoplasmic components during the oocyte-to-embryo transition (Danilchik and Denegre, 1991, Imoh, 1995). In 1991, Danilchik and Denegre hypothesized that this dramatic intracellular rearrangement during the oocyte-to-embryo transition might represent an important mechanism to regulate the functions of some maternal factors (Danilchik and Denegre, 1991). In agreement with this view, we found separation of the ubiquitin-independent proteasome from vegetally

localized germ plasm is important for germline development. It will be of interest to further study how this intracellular rearrangement occurs and prepares oocyte for embryonic development.

It is important to note that we do not understand the biological function of animally enriched proteasomes. During the oocyte-to-embryo transition, a series of important events happen in the animal hemisphere, including the completion of meiosis II and fusion of pronuclei. During cleavage, animal blastomeres divide slightly faster than vegetal blastomeres. It is possible that relocalization of the proteasome during the oocyte-to-embryo transition results in a higher protein turnover rate in the animal hemisphere, which facilitates some of these events. Interestingly, restriction of the proteasome to specific cellular compartment occurs during mouse oocyte-to-embryo transition as well. Before oocyte maturation, proteasomes are distributed in the germinal vesicle and cytoplasm of mouse oocytes. After fertilization, however, proteasomes become exclusively nuclear during cleavage. Proteasomes can be detected in the cytoplasm only when the blastocyst is formed (Evsikov et al., 2004, Solter et al., 2004). We speculate that relocalization of the proteasomes during the oocyte-to-embryo transition may be an evolutionarily conserved phenomenon. Future studies are needed to fully understand its biological function.

Methods and Materials

Xenopus laevis oocytes, embryos, and cell lines

In this work, we use *Xenopus laevis* oocytes, eggs, embryos for our investigation. All *Xenopus* procedures were approved by University of Illinois at Urbana-Champaign Institutional Animal Care and Use Committee (IACUC), under animal protocol # 17199 and performed in accordance with the recommendations of the Guide for the Care and Use of Laboratory Animals of the National Institutes of Health. Embryos were obtained as described (Sive et al., 2000). When performing microinjection, embryos were placed in 0.5xMMR with 3% Ficoll. In all experiments, we injected 10μl of solution into embryos using a Narishige IM300 microinjector. After injection, embryos were cultured in 0.2xMMR and harvested at desired stages. Stage VI oocytes were collected from an ovary by manual defolliculation (https://www.youtube.com/watch?v=us8rDNG69Sk) and cultured in oocyte culture medium (Heasman et al., 1994). Antisense oligo against *dnd1* was published (Mei et al., 2013, Aguero et al., 2017a). To induce oocyte maturation, oocytes were treated with progesterone (2 nM) overnight. Oocyte maturation was judged by the appearance of a white spot on the animal hemisphere of the oocyte. To induce artificial egg activation, eggs were pricked with a glass needle in the animal hemisphere. Eggs with obvious surface contraction were chosen to analyze further. We used Gastromaster (Nepagene, Japan) to dissect oocytes into animal and vegetal halves for RT-PCR analysis. All RNAs used for microinjection were synthesized from linearized plasmid templates using the mMESSAGE mMACHINE Kit (Ambion).

HEK293T and GC-2spd (Hofmann et al., 1994) cells were cultured in DMEM supplemented with 10% fetal bovine serum, penicillin, and streptomycin. Cells were cultured at 37 °C in a humidified, 5% CO_2 atmosphere. Transfection was performed using Lipofectamine 2000 as described (Jin et al., 2010).

Plasmids

GFP-myc-SV40 was described (Jin et al., 2009). To generate GFP-myc-*x.l.*dnd3'UTR, the 3'UTR of *Xenopus laevis dnd1* (Aguero et al., 2017a) was PCR amplified and cloned between the XhoI and NotI sites of GFP-myc-SV40. All other Dnd1 expression constructs used in this study were derived from *Xenopus tropicalis dnd1* (Mei et al., 2013) using standard PCR cloning methods. F110M and S117D were generated by site-directed mutagenesis from myc-Dnd1. Myc-RBM46 (IMAGE:7689323), myc-A1CF (IMAGE:3398290), and myc-hnRNP R (IMAGE:6316097) were generated by standard PCR cloning methods. pCS2-myc-Syncrip was cloned by RT-PCR using cDNA from stage 33 embryos. The ORFs of *psme1*, *psme2*, and *psme3* were PCR amplified from *Xenopus laevis* oocyte cDNA and cloned into pCS2 to generate pCS2-PSME1, pCS2-PSME2, and pCS2-PSME3. Dominant negative proteasome activator dnPSME1 (PSME1 N141Y), dnPSME2 (PSME2 N139Y), and dnPSME3 (PSME3 N151Y) (Zhang et al., 1998) were generated by site-directed mutagenesis. pCMV-SPORT6-PSME4 (IMAGE:6637082) was used for overexpression of PSME4. To generate dnPSME4, the BRDL region of PSME4 (residues 1635-1723) was PCR amplified and cloned into pCS2. Cloning details will be provided upon request.

Antibodies, western blots, and immunofluorescence

Antibodies used in this study include anti-myc (9E10, #5546, Sigma-Aldrich), anti-FLAG (M2, #F1804, Sigma-Aldrich), anti-β-tubulin (#T5293, Sigma-Aldrich), mouse anti-Hsc70 (Sc7298, Lot# C1716, Santa Cruz Biotechnology), rabbit anti-proteasome 20S core subunits (BML-PW8155-0100, Lot# 08081644, Enzo Life Sciences Inc.), rabbit anti-proteasome 20S α+β (ab22673, Lot# GR3218416, Abcam), and rabbit anti-Dnd1 (36).

Protocols for western blots were described previously (Jin et al., 2009). Briefly, oocytes or embryos were homogenized in NP40 lysis buffer (50mM Tris pH7.5, 125 mM NaCl, 1mM EDTA, 1% NP40) supplemented with protease inhibitor cocktails (Sigma, P8340) (40μl lysis buffer per oocyte or embryo). Lysates were cleared by centrifugation at 500 rcf for 5 minutes, then at the 20,000 rcf for 5 minutes. Cleared lysates were mixed with 2xSDS sample buffer, boiled for 3 minutes, and loaded on SDS-PAGE. Proteins were transferred to PVDF membrane for western blot according to the standard protocol. To detect endogenous Dnd1 by western blot, we enriched Dnd1 protein from 25 oocytes or embryos by immunoprecipitation before western blotting.

To detect proteasome 20S core particles by immunofluorescence, oocytes, eggs, and embryos (2-cell stage) were fixed with MEMFA, embedded in paraffin wax, and sectioned according to the standard protocol (Sive et al., 2000). For immuno-staining, sections were blocked with blocking buffer (0.2% BSA, 0.1 % Triton X-100 in 1xPBS) with 10% donkey serum for an hour at room temperature, and then stained with anti-proteasome 20S core subunits antibody (1:100) overnight. Sections were washed with blocking buffer three times and stained with goat anti-rabbit Alexa-555 fluorescent antibody (Invitrogen) for an hour. Samples were washed again with blocking buffer three times before mounting for imaging. We performed staining using two different antibodies (BML-PW8155-0100, Lot# 08081644, Enzo Life Sciences Inc.; ab22673, Lot# GR3218416, Abcam) and obtained essentially same staining results.

In situ hybridization and RT-PCR

For in situ hybridization, embryos and oocytes were fixed in MEMFA at room temperature for 1 hour, washed with PBS twice, and dehydrated in methanol. To assess the expression of proteasome components, we cut stage VI oocytes, ovulated eggs, and 2-cell stage embryos into halves using Razer blade. Hemi-sectioned oocytes, eggs, and 2-cell stage embryos were placed in the same vial for in hybridization as described (Rorick et al., 2007). Plasmids used for labeling *pgat* (Hudson and Woodland, 1998), *dnd1* (Aguero et al., 2017a) in situ probes are published. pCS2-PSME1, pCS2-PSME2, pCS2-PSME3, pCMV-SPORT6-PSME4, and EST clones TGas131c05, TEgg045c15, TGas116f12, and TTpA010e07 were used for making in situ probes for *psme1*, *psme2*, *psme3*, *psme4*, *psmc6*, *psma2*, *eIF4a1*, and *eIF4e*, respectively.

Real time PCR was performed using the SYBR® Green PCR Master Mix (Applied Biosystems) according to standard protocol (Aguero et al., 2017a). PCR primers include *odc* (Yang et al., 2003), *psme1* (5'-AGCTGAACTGGACATACCAATTCC-3'; 5'-CTCTTTTGATTCCTGGATTTCACTC-3'), *psme2* (5'-ATGTGGAGGACCTAGCAACC CTTC-3'; 5'-ATCCTTCTCTCAGGCTTCGTATCTC-3'), *psme3* (5'-CTGATTGAGAAGTGCAACACGG-3'; 5'-TGCTCTAGTGATGTAGTATCTGG-3'), and *psme4* (5'-GTGAGAAACAAAGCTCAGCAGGC-3'; 5'-CTGCACAATACACTCCCAGTCATGG-3').

Proteomic analysis of 1-cell stage embryo

Micropipettes were fabricated in-house and utilized for localized sample (cytoplasm) collection from *Xenopus laevis* embryos as per the protocol published in literature (Saha-Shah et al., 2015). Briefly, micropipettes were utilized to puncture the embryonic membrane and collect nanoliter volumes of cytoplasm *via* pressure actuation from the animal and vegetal hemispheres of individual embryos one hour post fertilization. The samples from animal and vegetal hemispheres were prepared separately for bottom-up mass spectrometry following standard protocols. Standard protocol includes treatment of the sample with dithiothreitol to reduce the proteins followed by alkylation of newly reduced thiols using iodoacetamide and finally digestion of the proteins to peptides using trypsin. The peptides were de-salted using c-18 stage tips prior to LC-MS/MS. A UltimateTM 3000 RSLCnano System nano liquid chromatography system was coupled to Q-Exactive™ HF-X Hybrid Quadrupole-Orbitrap™ Mass spectrometer (Thermo Scientific) for proteomic data acquisition. Proteomic data analysis was performed using Spectronaut™ 10 (Biognosys) software. The mass spectrometry data was searched using

Xenbase protein FASTA file (downloaded on September 2017). Proteomics data from five replicates or embryos were used of this study. Details of this method will be published separately in a manuscript under review (Saha-Shah et al., 2015).

Peptides abundances from LC-MS/MS data were log2 transformed, normalized by the average of the peptide abundance within each sample and finally raised to the power of 2 to reverse the initial log2 transformation. Protein abundance were obtained by averaging all detected peptides corresponding to a protein. Fig 6D plots the average of protein abundance across all conditions and replicates in the y-axis against Log_2 of protein abundance ratio between animal and vegetal hemispheres. All proteins were quantified with >2 peptides. Raw LC-MS files can be found in Chorus repository, project ID 1556.

Acknowledgements

We thank Dr. Romana Nowak for providing GC-2spd cells. MLK (R01GM102397), MW (R03AI138138), PK (1R01GM115517 and 1R01HL141759) and JY (R01GM111816) are supported by grants from National Institute of Health.

Author contributions

Conceptualization: H.H., Z.J., J.Y.; Methodology: H.H, Z.J., V.V.K., A.S., P.K., B.G., W.M., K.Z., J.Y.; Validation: H.H, Z.J.; Investigation: H.H, Z.J., V.V.K., A.S., W.M., J.Y.; Data analysis: H.H, Z.J.; V.V.K., A.S., P.K., B.G., M.L.K., K.Z., J.Y.; Writing - original draft: J.Y.; Writing - review & editing: M.L.K., J.Y.; Supervision: J.Y.; Project administration: J.Y.; Funding acquisition: W.M., M.L.K., J.Y.

References

AGUERO, T., JIN, Z., CHORGHADE, S., KALSOTRA, A., KING, M. L. & YANG, J. 2017a. Maternal Dead-end 1 promotes translation of nanos1 by binding the eIF3 complex. *Development,* 144**,** 3755-3765.

AGUERO, T., JIN, Z., OWENS, D., MALHOTRA, A., NEWMAN, K., YANG, J. & KING, M. L. 2018. Combined functions of two RRMs in Dead-end1 mimic helicase activity to promote nanos1 translation in the germline. *Mol Reprod Dev,* 85**,** 896-908.

AGUERO, T., KASSMER, S., ALBERIO, R., JOHNSON, A. & KING, M. L. 2017b. Mechanisms of Vertebrate Germ Cell Determination. *Adv Exp Med Biol,* 953**,** 383-440.

BEN-NISSAN, G. & SHARON, M. 2014. Regulating the 20S proteasome ubiquitin-independent degradation pathway. *Biomolecules,* 4**,** 862-84.

BOWERMAN, B. & KURZ, T. 2006. Degrade to create: developmental requirements for ubiquitin-mediated proteolysis during early C. elegans embryogenesis. *Development,* 133**,** 773-84.

BUTLER, A. M., OWENS, D. A., WANG, L. & KING, M. L. 2018. A novel role for sox7 in Xenopus early primordial germ cell development: mining the PGC transcriptome. *Development,* 145.

COOK, M. S., COVENEY, D., BATCHVAROV, I., NADEAU, J. H. & CAPEL, B. 2009. BAX-mediated cell death affects early germ cell loss and incidence of testicular teratomas in Dnd1(Ter/Ter) mice. *Dev Biol,* 328**,** 377-83.

CUYKENDALL, T. N. & HOUSTON, D. W. 2009. Vegetally localized Xenopus trim36 regulates cortical rotation and dorsal axis formation. *Development,* 136**,** 3057-65.

DANILCHIK, M. V. & DENEGRE, J. M. 1991. Deep cytoplasmic rearrangements during early development in Xenopus laevis. *Development,* 111**,** 845-56.

DERENZO, C. & SEYDOUX, G. 2004. A clean start: degradation of maternal proteins at the oocyte-to-embryo transition. *Trends Cell Biol,* 14**,** 420-6.

DESHPANDE, G., CALHOUN, G., YANOWITZ, J. L. & SCHEDL, P. D. 1999. Novel functions of nanos in downregulating mitosis and transcription during the development of the Drosophila germline. *Cell,* 99**,** 271-81.

EVSIKOV, A. V., DE VRIES, W. N., PEASTON, A. E., RADFORD, E. E., FANCHER, K. S., CHEN, F. H., BLAKE, J. A., BULT, C. J., LATHAM, K. E., SOLTER, D. & KNOWLES, B. B. 2004. Systems biology of the 2-cell mouse embryo. *Cytogenet Genome Res,* 105**,** 240-50.

EXTAVOUR, C. G. & AKAM, M. 2003. Mechanisms of germ cell specification across the metazoans: epigenesis and preformation. *Development,* 130**,** 5869-84.

GROSS-THEBING, T., YIGIT, S., PFEIFFER, J., REICHMAN-FRIED, M., BANDEMER, J., RUCKERT, C., RATHMER, C., GOUDARZI, M., STEHLING, M., TARBASHEVICH, K., SEGGEWISS, J. & RAZ, E. 2017. The Vertebrate Protein Dead End Maintains Primordial Germ Cell Fate by Inhibiting Somatic Differentiation. *Dev Cell,* 43**,** 704-715 e5.

HEASMAN, J., CRAWFORD, A., GOLDSTONE, K., GARNER-HAMRICK, P., GUMBINER, B., MCCREA, P., KINTNER, C., NORO, C. Y. & WYLIE, C. 1994. Overexpression of cadherins and underexpression of beta-catenin inhibit dorsal mesoderm induction in early Xenopus embryos. *Cell,* 79**,** 791-803.

HOFMANN, M. C., HESS, R. A., GOLDBERG, E. & MILLAN, J. L. 1994. Immortalized germ cells undergo meiosis in vitro. *Proc Natl Acad Sci U S A,* 91**,** 5533-7.

HORVAY, K., CLAUSSEN, M., KATZER, M., LANDGREBE, J. & PIELER, T. 2006. Xenopus Dead end mRNA is a localized maternal determinant that serves a conserved function in germ cell development. *Dev Biol,* 291**,** 1-11.

HOUSTON, D. W. & KING, M. L. 2000. A critical role for Xdazl, a germ plasm-localized RNA, in the differentiation of primordial germ cells in Xenopus. *Development,* 127**,** 447-56.

HOUSTON, D. W., ZHANG, J., MAINES, J. Z., WASSERMAN, S. A. & KING, M. L. 1998. A Xenopus DAZ-like gene encodes an RNA component of germ plasm and is a functional homologue of Drosophila boule. *Development,* 125**,** 171-80.

HOYT, M. A. & COFFINO, P. 2004. Ubiquitin-free routes into the proteasome. *Cell Mol Life Sci,* 61**,** 1596-600.

HUANG, L., HARATAKE, K., MIYAHARA, H. & CHIBA, T. 2016. Proteasome activators, PA28gamma and PA200, play indispensable roles in male fertility. *Sci Rep,* 6**,** 23171.

HUDSON, C. & WOODLAND, H. R. 1998. Xpat, a gene expressed specifically in germ plasm and primordial germ cells of Xenopus laevis. *Mech Dev,* 73**,** 159-68.

HWANG, J., WINKLER, L. & KALEJTA, R. F. 2011. Ubiquitin-independent proteasomal degradation during oncogenic viral infections. *Biochim Biophys Acta,* 1816**,** 147-57.

IMOH, H. 1995. Establishment and movement of egg regions revealed by the size class of yolk platelets in Xenopus laevis. *Roux Arch Dev Biol,* 205**,** 128-137.

IRIE, N., WEINBERGER, L., TANG, W. W., KOBAYASHI, T., VIUKOV, S., MANOR, Y. S., DIETMANN, S., HANNA, J. H. & SURANI, M. A. 2015. SOX17 is a critical specifier of human primordial germ cell fate. *Cell,* 160**,** 253-68.

JARUZELSKA, J., KOTECKI, M., KUSZ, K., SPIK, A., FIRPO, M. & REIJO PERA, R. A. 2003. Conservation of a Pumilio-Nanos complex from Drosophila germ plasm to human germ cells. *Dev Genes Evol,* 213**,** 120-6.

JIN, Z., SHI, J., SARAF, A., MEI, W., ZHU, G. Z., STRACK, S. & YANG, J. 2009. The 48-kDa alternative translation isoform of PP2A:B56epsilon is required for Wnt signaling during midbrain-hindbrain boundary formation. *J Biol Chem,* 284**,** 7190-200.

JIN, Z., WALLACE, L., HARPER, S. Q. & YANG, J. 2010. PP2A:B56{epsilon}, a substrate of caspase-3, regulates p53-dependent and p53-independent apoptosis during development. *J Biol Chem,* 285**,** 34493-502.

KARABINOVA, P., KUBELKA, M. & SUSOR, A. 2011. Proteasomal degradation of ubiquitinated proteins in oocyte meiosis and fertilization in mammals. *Cell Tissue Res,* 346**,** 1-9.

KEDDE, M., STRASSER, M. J., BOLDAJIPOUR, B., OUDE VRIELINK, J. A., SLANCHEV, K., LE SAGE, C., NAGEL, R., VOORHOEVE, P. M., VAN DUIJSE, J., OROM, U. A., LUND, A. H., PERRAKIS, A., RAZ, E. & AGAMI, R. 2007. RNA-binding protein Dnd1 inhibits microRNA access to target mRNA. *Cell,* 131**,** 1273-86.

KHOR, B., BREDEMEYER, A. L., HUANG, C. Y., TURNBULL, I. R., EVANS, R., MAGGI, L. B., JR., WHITE, J. M., WALKER, L. M., CARNES, K., HESS, R. A. & SLECKMAN, B. P. 2006. Proteasome activator PA200 is required for normal spermatogenesis. *Mol Cell Biol,* 26**,** 2999-3007.

KISH-TRIER, E. & HILL, C. P. 2013. Structural biology of the proteasome. *Annu Rev Biophys,* 42**,** 29-49.

KLOC, M., BILINSKI, S., CHAN, A. P., ALLEN, L. H., ZEARFOSS, N. R. & ETKIN, L. D. 2001. RNA localization and germ cell determination in Xenopus. *Int Rev Cytol,* 203**,** 63-91.

KLOC, M. & ETKIN, L. D. 2005. RNA localization mechanisms in oocytes. *J Cell Sci,* 118**,** 269-82.

KOEBERNICK, K., LOEBER, J., ARTHUR, P. K., TARBASHEVICH, K. & PIELER, T. 2010. Elr-type proteins protect Xenopus Dead end mRNA from miR-18-mediated clearance in the soma. *Proc Natl Acad Sci U S A,* 107**,** 16148-53.

LAI, F., SINGH, A. & KING, M. L. 2012. Xenopus Nanos1 is required to prevent endoderm gene expression and apoptosis in primordial germ cells. *Development,* 139**,** 1476-86.

LAI, F., ZHOU, Y., LUO, X., FOX, J. & KING, M. L. 2011. Nanos1 functions as a translational repressor in the Xenopus germline. *Mech Dev,* 128**,** 153-63.

LAWSON, K. A., DUNN, N. R., ROELEN, B. A., ZEINSTRA, L. M., DAVIS, A. M., WRIGHT, C. V., KORVING, J. P. & HOGAN, B. L. 1999. Bmp4 is required for the generation of primordial germ cells in the mouse embryo. *Genes Dev,* 13**,** 424-36.

LI, Q., LI, Y., YANG, S., HUANG, S., YAN, M., DING, Y., TANG, W., LOU, X., YIN, Q., SUN, Z., LU, L., SHI, H., WANG, H., CHEN, Y. & LI, J. 2018. CRISPR-Cas9-mediated base-editing screening in mice identifies DND1 amino acids that are critical for primordial germ cell development. *Nat Cell Biol,* 20**,** 1315-1325.

LUO, X., NERLICK, S., AN, W. & KING, M. L. 2011. Xenopus germline nanos1 is translationally repressed by a novel structure-based mechanism. *Development,* 138**,** 589-98.

MEI, W., JIN, Z., LAI, F., SCHWEND, T., HOUSTON, D. W., KING, M. L. & YANG, J. 2013. Maternal Dead-End1 is required for vegetal cortical microtubule assembly during Xenopus axis specification. *Development,* 140**,** 2334-44.

MULLER, S. & SCHWARTZ, L. M. 1995. Ubiquitin in homeostasis, development and disease. *Bioessays,* 17**,** 677-84.

MURATA, S., UDONO, H., TANAHASHI, N., HAMADA, N., WATANABE, K., ADACHI, K., YAMANO, T., YUI, K., KOBAYASHI, N., KASAHARA, M., TANAKA, K. & CHIBA, T. 2001. Immunoproteasome assembly and antigen presentation in mice lacking both PA28alpha and PA28beta. *EMBO J,* 20**,** 5898-907.

NAKAHATA, S., KATSU, Y., MITA, K., INOUE, K., NAGAHAMA, Y. & YAMASHITA, M. 2001. Biochemical identification of Xenopus Pumilio as a sequence-specific cyclin B1 mRNA-binding protein that physically interacts with a Nanos homolog, Xcat-2, and a cytoplasmic polyadenylation element-binding protein. *J Biol Chem,* 276**,** 20945-53.

OHINATA, Y., OHTA, H., SHIGETA, M., YAMANAKA, K., WAKAYAMA, T. & SAITOU, M. 2009. A signaling principle for the specification of the germ cell lineage in mice. *Cell,* 137**,** 571-84.

QIAN, M. X., PANG, Y., LIU, C. H., HARATAKE, K., DU, B. Y., JI, D. Y., WANG, G. F., ZHU, Q. Q., SONG, W., YU, Y., ZHANG, X. X., HUANG, H. T., MIAO, S., CHEN, L. B., ZHANG, Z. H., LIANG, Y. N., LIU, S., CHA, H., YANG, D., ZHAI, Y., KOMATSU, T., TSURUTA, F., LI, H., CAO, C., LI, W., LI, G. H., CHENG, Y., CHIBA, T., WANG, L., GOLDBERG, A. L., SHEN, Y. & QIU, X. B. 2013. Acetylation-mediated proteasomal degradation of core histones during DNA repair and spermatogenesis. *Cell,* 153**,** 1012-24.

RECHSTEINER, M. & HILL, C. P. 2005. Mobilizing the proteolytic machine: cell biological roles of proteasome activators and inhibitors. *Trends Cell Biol,* 15**,** 27-33.

RORICK, A. M., MEI, W., LIETTE, N. L., PHIEL, C., EL-HODIRI, H. M. & YANG, J. 2007. PP2A:B56epsilon is required for eye induction and eye field separation. *Dev Biol,* 302**,** 477-493.

SAHA-SHAH, A., WEBER, A. E., KARTY, J. A., RAY, S. J., HIEFTJE, G. M. & BAKER, L. A. 2015. Nanopipettes: probes for local sample analysis. *Chem Sci,* 6**,** 3334-3341.

SAITOU, M. 2009. Germ cell specification in mice. *Curr Opin Genet Dev,* 19**,** 386-95.

SATO, K., HAYASHI, Y., NINOMIYA, Y., SHIGENOBU, S., ARITA, K., MUKAI, M. & KOBAYASHI, S. 2007. Maternal Nanos represses hid/skl-dependent apoptosis to maintain the germ line in Drosophila embryos. *Proc Natl Acad Sci U S A,* 104**,** 7455-60.

SCHANER, C. E., DESHPANDE, G., SCHEDL, P. D. & KELLY, W. G. 2003. A conserved chromatin architecture marks and maintains the restricted germ cell lineage in worms and flies. *Dev Cell,* 5**,** 747-57.

SEYDOUX, G. & BRAUN, R. E. 2006. Pathway to totipotency: lessons from germ cells. *Cell,* 127**,** 891-904.

SINDELKA, R., ABAFFY, P., QU, Y., TOMANKOVA, S., SIDOVA, M., NARAINE, R., KOLAR, M., PEUCHEN, E., SUN, L., DOVICHI, N. & KUBISTA, M. 2018. Asymmetric distribution of biomolecules of maternal origin in the Xenopus laevis egg and their impact on the developmental plan. *Sci Rep,* 8**,** 8315.

SIVE, H., GRAINGER, R. & HARLAND, R. 2000. *Early Development of Xenopus laevis; A Laboratory Manual,* Cold Spring Harbor, Cold Spring Harbor Press.

SOLTER, D., HIIRAGI, T., EVSIKOV, A. V., MOYER, J., DE VRIES, W. N., PEASTON, A. E. & KNOWLES, B. B. 2004. Epigenetic mechanisms in early mammalian development. *Cold Spring Harb Symp Quant Biol,* 69**,** 11-7.

SONODA, J. & WHARTON, R. P. 1999. Recruitment of Nanos to hunchback mRNA by Pumilio. *Genes Dev,* 13**,** 2704-12.
SONODA, J. & WHARTON, R. P. 2001. Drosophila Brain Tumor is a translational repressor. *Genes Dev,* 15**,** 762-73.
STROME, S. & LEHMANN, R. 2007. Germ versus soma decisions: lessons from flies and worms. *Science,* 316**,** 392-3.
TAM, P. P. & ZHOU, S. X. 1996. The allocation of epiblast cells to ectodermal and germ-line lineages is influenced by the position of the cells in the gastrulating mouse embryo. *Dev Biol,* 178**,** 124-32.
TSUKAMOTO, S. & TATSUMI, T. 2018. Degradation of maternal factors during preimplantation embryonic development. *J Reprod Dev,* 64**,** 217-222.
WEIDINGER, G., STEBLER, J., SLANCHEV, K., DUMSTREI, K., WISE, C., LOVELL-BADGE, R., THISSE, C., THISSE, B. & RAZ, E. 2003. dead end, a novel vertebrate germ plasm component, is required for zebrafish primordial germ cell migration and survival. *Curr Biol,* 13**,** 1429-34.
WONG, E. & CUERVO, A. M. 2010. Integration of clearance mechanisms: the proteasome and autophagy. *Cold Spring Harb Perspect Biol,* 2**,** a006734.
WYLIE, C. 1999. Germ cells. *Cell,* 96**,** 165-74.
YANG, J., AGUERO, T. & KING, M. L. 2015. The Xenopus Maternal-to-Zygotic Transition from the Perspective of the Germline. *Curr Top Dev Biol,* 113**,** 271-303.
YANG, J., WU, J., TAN, C. & KLEIN, P. S. 2003. PP2A:B56epsilon is required for Wnt/beta-catenin signaling during embryonic development. *Development,* 130**,** 5569-78.
YING, Y., QI, X. & ZHAO, G. Q. 2001. Induction of primordial germ cells from murine epiblasts by synergistic action of BMP4 and BMP8B signaling pathways. *Proc Natl Acad Sci U S A,* 98**,** 7858-62.
YOUNGREN, K. K., COVENEY, D., PENG, X., BHATTACHARYA, C., SCHMIDT, L. S., NICKERSON, M. L., LAMB, B. T., DENG, J. M., BEHRINGER, R. R., CAPEL, B., RUBIN, E. M., NADEAU, J. H. & MATIN, A. 2005. The Ter mutation in the dead end gene causes germ cell loss and testicular germ cell tumours. *Nature,* 435**,** 360-4.
ZHANG, Z., REALINI, C., CLAWSON, A., ENDICOTT, S. & RECHSTEINER, M. 1998. Proteasome activation by REG molecules lacking homolog-specific inserts. *J Biol Chem,* 273**,** 9501-9.
ZHOU, Y. & KING, M. L. 1996. Localization of Xcat-2 RNA, a putative germ plasm component, to the mitochondrial cloud in Xenopus stage I oocytes. *Development,* 122**,** 2947-53.

Figures

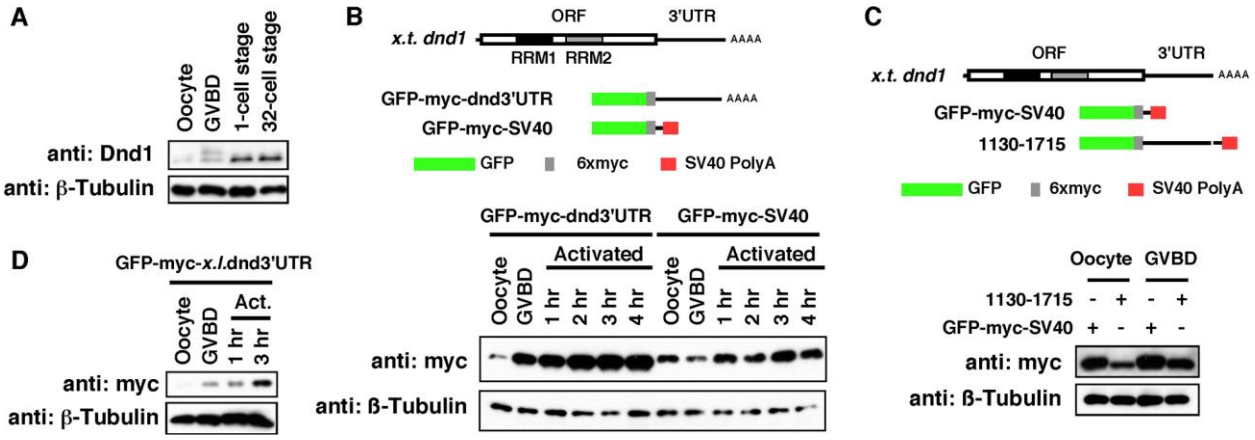

Figure 1. *dnd1* translation is repressed in the oocyte. (A) Western blot analysis showing the expression of endogenous Dnd1 in fully-grown oocytes, matured eggs (GVBD), fertilized eggs (1-cell stage), and 32-cell stage embryos. Experiments were performed for three times. **(B)** The activity of *Xenopus tropicalis dnd1* 3'UTR in directing translation of GFP. Upper panel is schematic diagram of *Xenopus tropicalis dnd1*, GFP-myc-dnd3'UTR, and GFP-myc-SV40. Western blot in lower panel shows the expression of GFP-myc-dnd3'UTR, and GFP-myc-SV40 in oocytes, matured eggs, and eggs artificially activated by needle pricking. Experiments were repeated for four times. **(C)** Western blot analysis showing *dnd1* 3'UTR contains inhibitory element(s) that suppresses translation of GFP-myc-SV40 in the oocyte, but not after oocyte maturation. Upper panel is a schematic diagram of *Xenopus tropicalis dnd1*, GFP-myc-SV40, and 1130-1751. ß-tubulin served as the loading control. Experiments were repeated for three times. **(D)** Activity of *Xenopus laevis dnd1* 3'UTR in directing translation of GFP in oocytes, matured eggs, and artificially activated eggs (Act.). Experiments were repeated for three times.

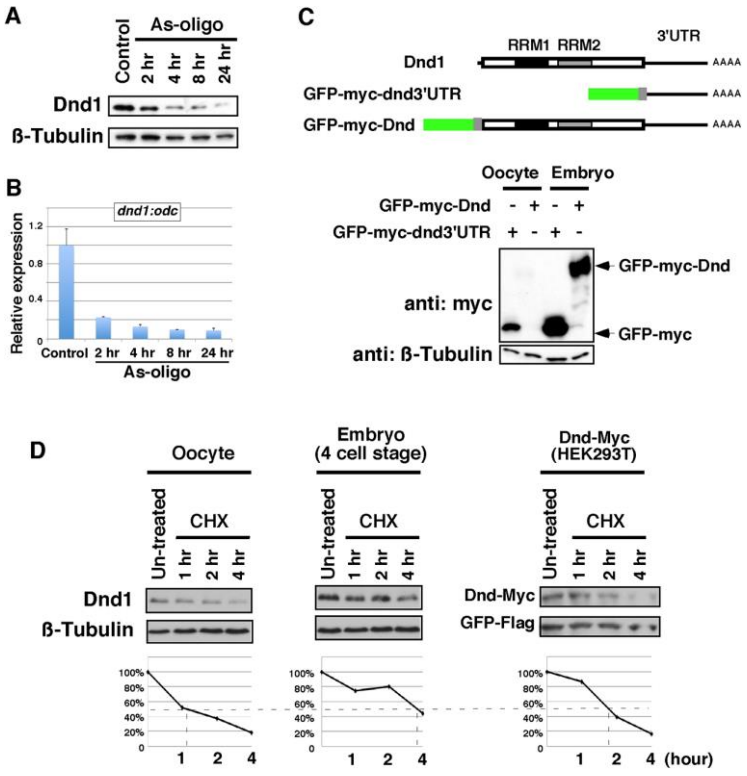

Figure 2. Dnd1 is intrinsically unstable in the oocyte. The level of Dnd1 protein **(A)** and *dnd1* mRNA (**B**) in control and *dnd1* As-oligo (10 ng) injected oocytes. Injected oocytes were harvested at 2, 4, 8, and 24 hours post As-oligo injection and analyzed by western blot (**A**) and real-time RT-PCR **(B)**. Experiments were performed twice. **(C)** Western blot results showing the expression of GFP and GFP-Dnd1 protein in oocytes and embryos. Upper panel is a schematic diagram of Dnd1, GFP-myc-dnd3'UTR, and GFP-myc-Dnd1. Both GFP-myc-dnd3'UTR and GFP-myc-Dnd1 constructs contain the 3'UTR of *dnd1*. Experiments were repeated for four times. **(D)** Protein synthesis in *Xenopus* oocytes, embryos, and Dnd1-myc transfected HEK293T cells was blocked by CHX treatment. We treated embryos with CHX from the 4-cell stage. Samples were harvested at multiple time points after addition of CHX and analyzed by western blot. Proteins bands were quantified using ImageJ and plotted into graphs. Experiments were performed twice.

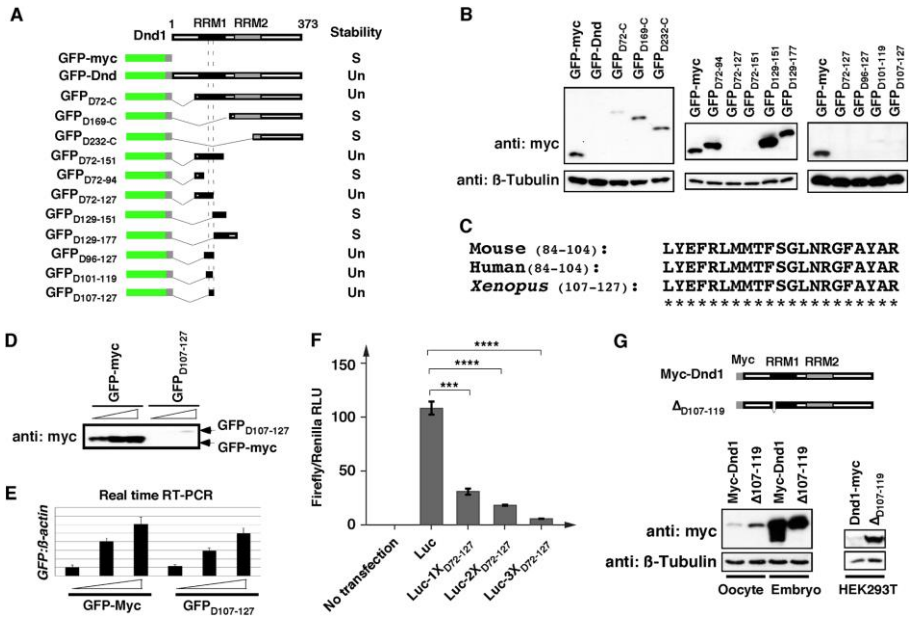

Figure 3. Identification the degron that mediates Dnd1 turnover in the oocyte. (A) Schematic diagram of various Dnd1-GFP fusion constructs used for mapping the degron that mediates Dnd1 turnover in the oocyte. Whether a construct is **s**table or **un**stable in the oocyte is summarized on the right side. **(B)** Western blot showing the expression of various Dnd1-GFP fusion constructs in the oocyte. Experiments were performed three times. **(C)** The sequence of degron D107-127 is conserved from *Xenopus* to human. **(D** and **E)** GFP-myc and $GFP_{D107-127}$ were transfected into HEK293T cells. The protein **(D)** and mRNA (**E**) expression levels of GFP-myc and $GFP_{D107-127}$ were monitored by western blot and real-time RT-PCR, respectively. Experiments were performed twice. **(F)** Dual luciferase assay showing destabilization of luciferase by degron D107-127 in NIH3T3 cells. Luciferase activities were normalized to that of the Renilla luciferase. Two-tailed *t*-tests were performed. ***p<0.001; ****p<0.0001. (**G**) Western blot showing the expression of the full-length Dnd1 and $\Delta_{D107-119}$ in *Xenopus* oocytes, embryos, and HEK293T cells. ß-tubulin in **B** and **G** served as loading controls. Experiments were repeated for four times.

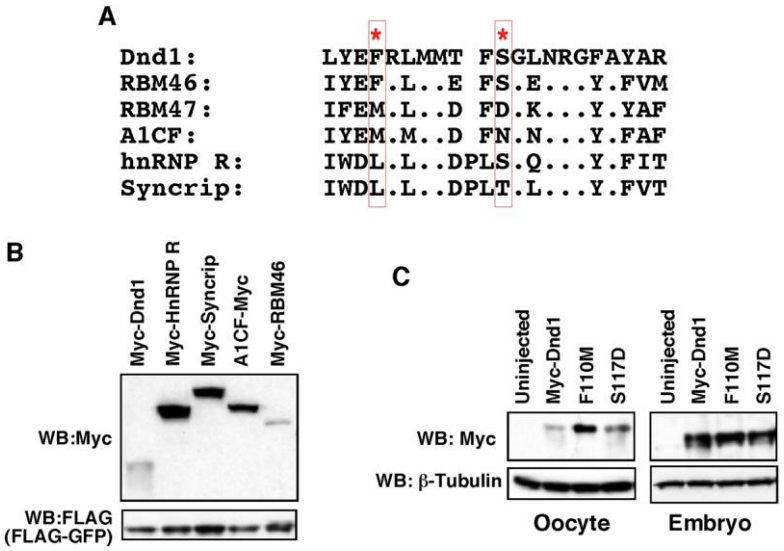

Figure 4. Characterization of degron D107-127. (A) Identification of *Xenopus* proteins containing a motif similar to degron D107-127. **(B)** Myc-Dnd1, myc-hnRNP R, myc-Syncrip, A1CF-myc, and myc-RBM46 were transfected into HEK293T cells. The expression of these constructs was monitored by western blot. Experiments were repeated for three times. **(C)** Western blot showing the expression of Myc-Dnd1, F110M, and S117D in *Xenopus* oocytes and embryos. Experiments were performed four times.

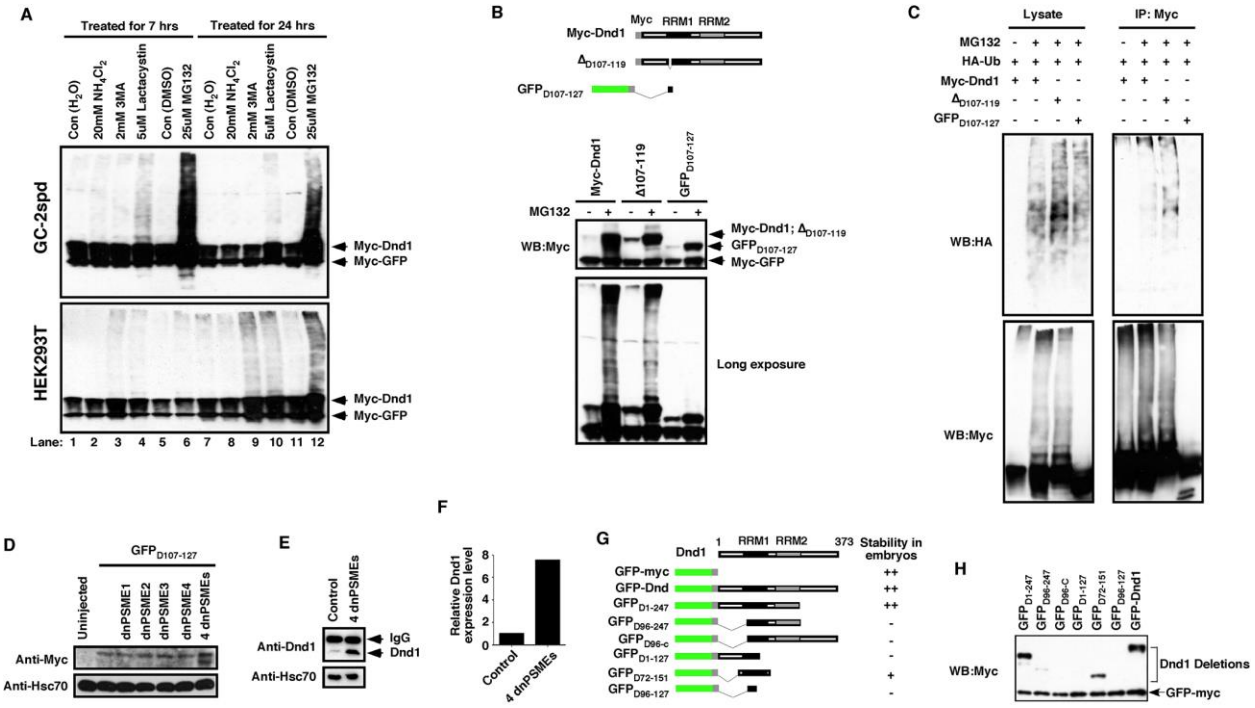

Figure 5. Degron D107-127 targets Dnd1 to the ubiquitin-independent proteasome degradation pathway. (A) Myc-Dnd1 and myc-GFP were transfected into GC-2spd and HEK293T cells. Transfected cells were treated with various inhibitors for 7 and 24 hours. Western blot was performed to monitor the expression of myc-Dnd1. Experiments were performed three times. **(B)** Western blot analysis showing effects of MG132 on the expression of myc-Dnd1, $\Delta_{D107-119}$, and $GFP_{D107-127}$. Experiments were performed three times. **(C)** Myc-Dnd1, $\Delta_{D107-119}$, and $GFP_{D107-127}$ were co-transfected with HA-ubiquitin. Cells were treated with MG132 to prevent proteasomal degradation of proteins. Myc-Dnd1, $\Delta_{D107-119}$, and $GFP_{D107-127}$ were immunoprecipitated using an anti-myc antibody and analyzed by western blot. Experiments were performed twice. **(D)** Western blot showing that overexpression of dominant negative proteasome activators individually had no effects on the expression of $GFP_{D107-127}$ in *Xenopus* oocytes. $GFP_{D107-127}$ was stabilized by coexpression of all four dnPSMEs. Experiments were performed three times. **(E)** Co-expression of all four dominant negative proteasome activators

stabilized endogenous Dnd1 in *Xenopus* oocytes. RNAs encoding dnPSME1, dnPSME2, dnPSME3, and dnPSME4 (2.5 ng each) was injected into the vegetal pole of oocytes. Oocytes were cultured for 20 hours after injection and then harvested for IP/western blot analysis. Experiments were repeated for four times. **(F)** Dnd1 proteins bands in **E** were quantified using ImageJ and plotted into graphs. **(G)** Schematic diagram of various Dnd1-GFP fusion constructs. The stability of each construct in *Xenopus* embryos is summarized on the right side of the construct. **(H)** Western blot showing the expression of Dnd1-GFP fusion constructs in *Xenopus* embryos. RNA encoding GFP-myc was co-injected with Dnd1-GFP fusion constructs as a control for injection and loading. Experiments were performed three times.

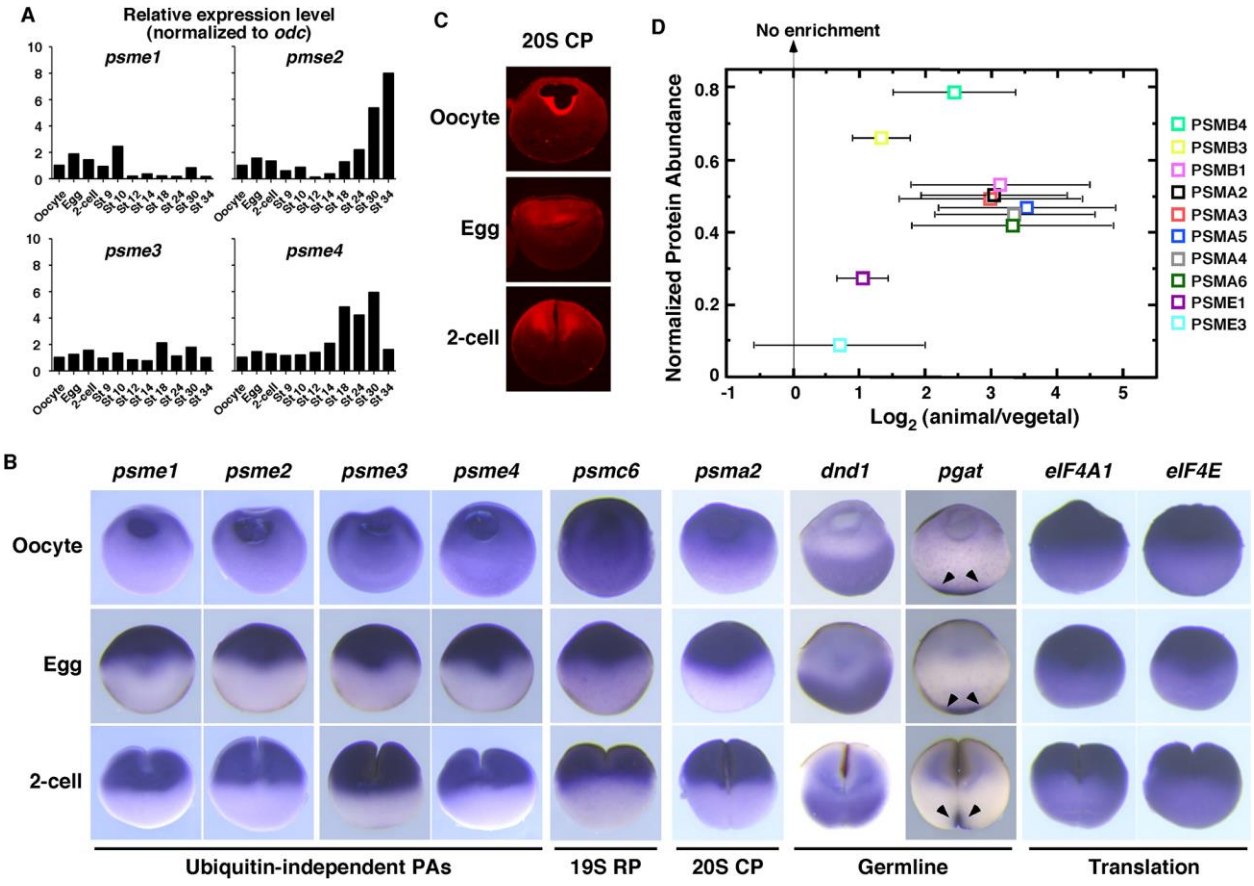

Figure 6. Vegetal-to-animal translocation of proteasome during the oocyte-to-embryo transition. (A) Real-time RT-PCR showing the expression of *psme1, psme2, psme3,* and *psme4* during *Xenopus* development. **(B)** In situ hybridization showing the expression of *psme1, psme2, psme3, psme4, psmc6, psma2, dnd1, pgat, eIF4A1,* and *eIF4E* in hemi-sectioned oocytes, ovulated eggs, embryos at 2-cell stage. Images shown here are representative images from at least 15 samples. **(C)** Immunofluorescence showing the subcellular distribution of 20S CP in oocytes, ovulated eggs, embryos at 2-cell stage. We stained oocytes, eggs, and embryos with two different anti-proteasome 20S CP antibodies (BML-PW8155-0100, Lot# 08081644, Enzo Life Sciences Inc.; ab22673, Lot# GR3218416, Abcam) and obtained essentially the same results. Results shown here, which were obtained using the antibody from Enzo Life Sciences Inc, were

representative images from 23 samples. **(D)** Quantification of proteasome components in the animal and vegetal hemispheres of 1-cell stage embryo by mass spectrometry. The histogram shows the average of protein abundance across all conditions and replicates in the y-axis against Log_2 of protein abundance ratio between animal and vegetal hemispheres. Of note, higher abundance of proteins enables more confident quantifications. n=5 replicates of animal and vegetal. Error bar corresponds to standard error of mean (SEM).

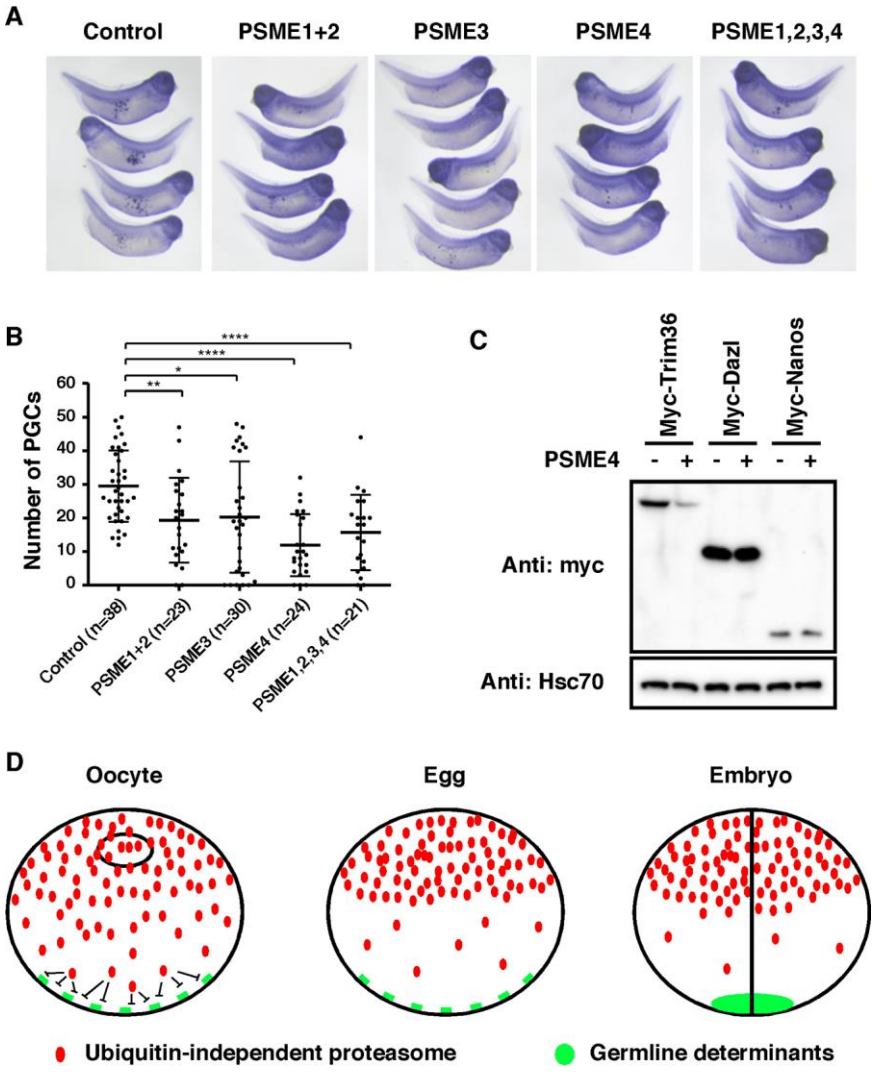

Figure 7. Ubiquitin-independent proteasomes inhibit germline development. (A) In situ hybridization showing the expression of *pgat* in control, and embryos injected with *psme1+psme2*, *psme3*, *psme4*, and all four *psme* RNAs. RNAs were injection into the vegetal pole at the 1-cell stage. **(B)** Quantification of results shown in **A**. The number of *pgat*-positive PGCs from each embryo was counted and plotted on the graph. Two-tailed *t*-tests were performed. *p<0.05; **p<0.01; ****p<0.0001. **(C)** Western blot showing that overexpression of PSME4 reduced the expression of myc-Trim36, but not myc-Dazl or myc-Nanos1. Hsc70 served as a loading control. Experiments were performed four times. **(D)** Working hypothesis of ubiquitin-independent proteasome function in controlling germline development. Ubiquitin-

independent proteasome forms an animal-to-vegetal gradient in fully-grown oocytes. In the vegetal hemisphere, it promotes degradation of germline determinants such as Dnd1. During the oocyte-to-embryo, RNAs coding for proteasome components are translocated to the animal hemisphere. Consequently, the proteasomal degradation rate is decreased in the vegetal hemisphere of the embryo. Reduced protein turnover in the vegetal pole creates a permissive environment, allowing rapid accumulation of germline determinants, which facilitates PGC development.

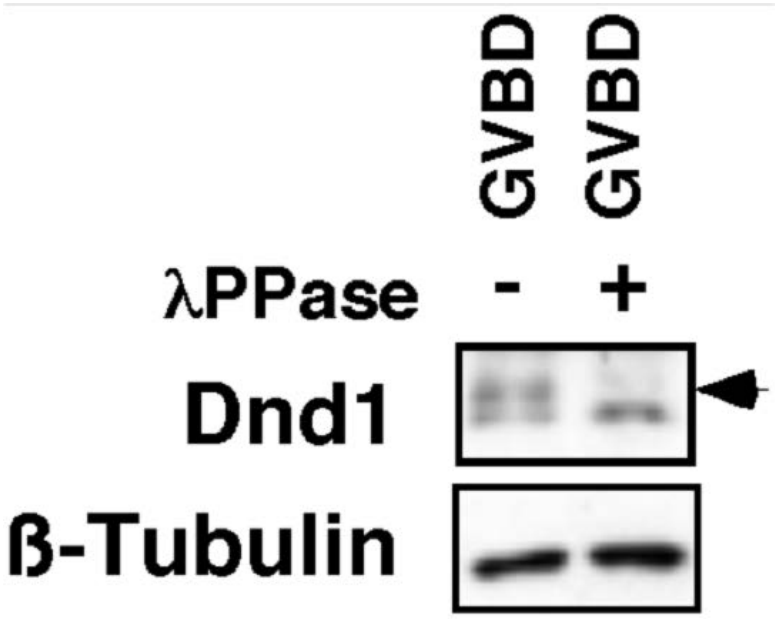

Figure S1. Phosphorylation of Dnd1 after oocyte maturation. (A) Western blot analysis showing the expression of endogenous Dnd1 in eggs (GVBD). Endogenous Dnd1 was enriched by IP from 50 eggs. Half of the IP sample was treated with λPPase. Arrow points to a band detected by anti-Dnd1 antibody, which migrates on SDS-PAGE relatively slowly. This band collapsed after phosphatase treatment, demonstrating that this is a phosphorylated form of Dnd1.

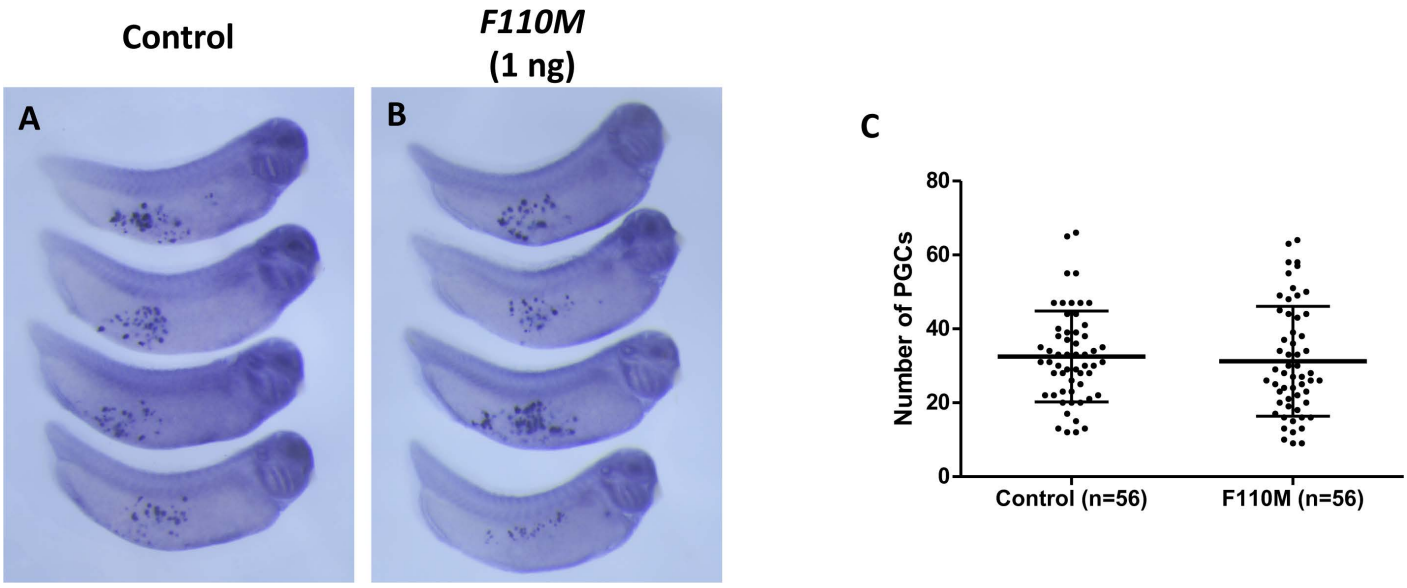

Figure S2. Overexpression of F110M had no effect on PGC development. (A) In situ hybridization showing the expression of *pgat* in control, and *F110M* (1 ng) injected embryos. RNA was injection into the vegetal pole at the 1-cell stage. **(B)** Quantification of results shown in **A**. The number of *pgat*-positive PGCs from each embryo was counted and plotted on the graph. There is no statistically significant difference between control and F110M overexpressed embryos.

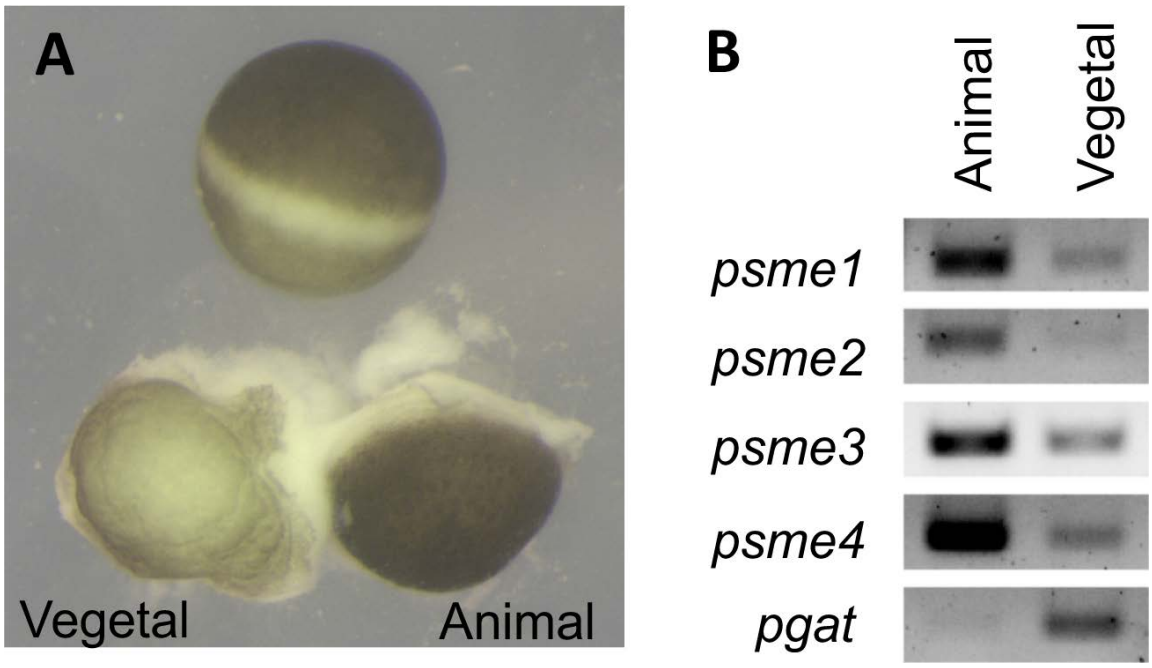

Figure S3. Asymmetric distribution of RNAs encoding ubiquitin-independent proteasome activator. (A) An intact stage VI oocyte and an oocyte that was dissected into animal and vegetal halves. **(B)** RT-PCR results showing the expression of *psme1*, *psme2*, *psme3*, *psme4*, and *pgat* in animal and vegetal halves of dissected oocytes. *pgat* was used as a marker for the vegetal hemisphere.

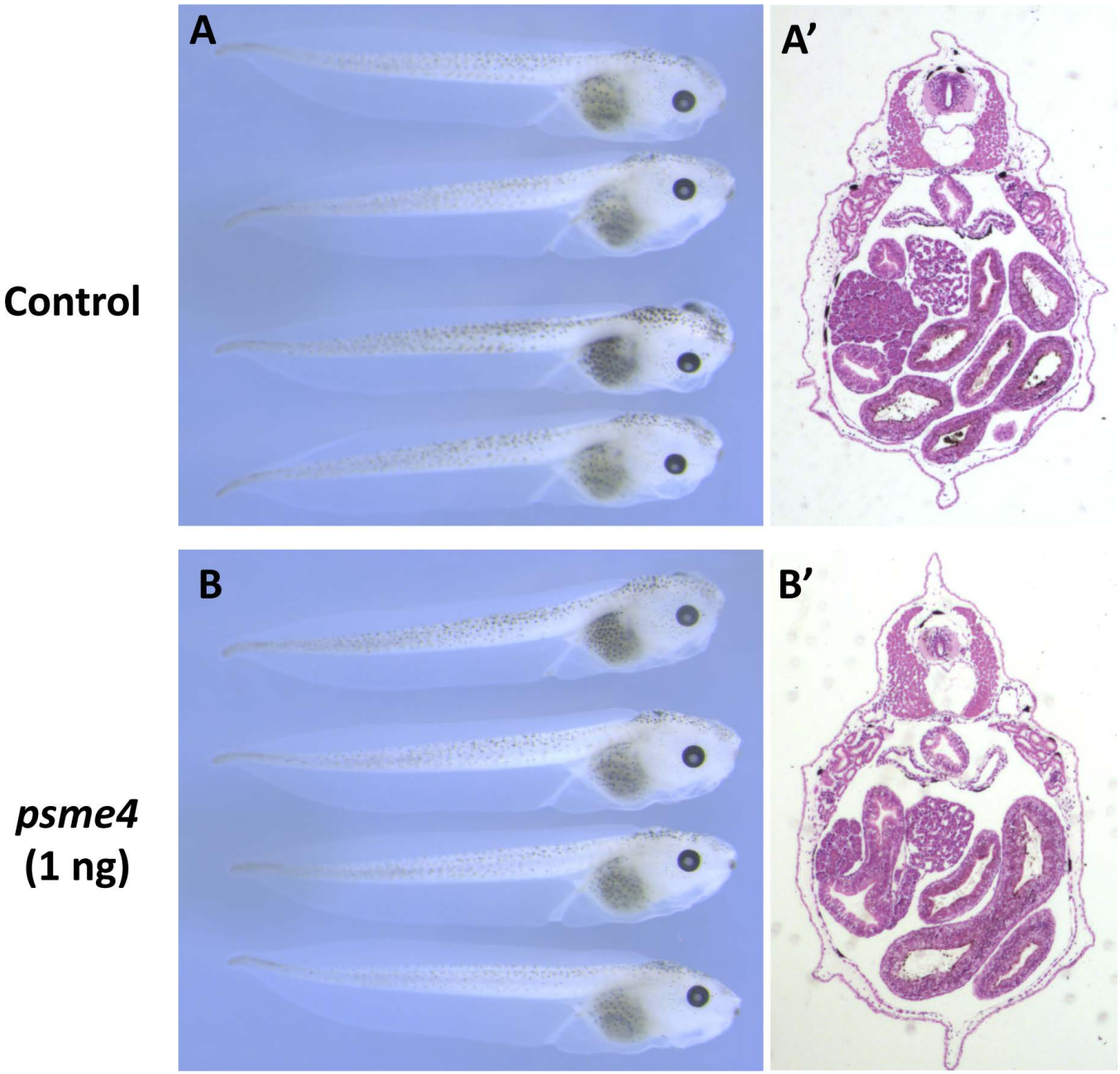

Figure S4. Overexpression of PSME4 had no effect on somatic development. Whole embryo morphology **(A** and **B)** and cross-section **(A'** and **B')** of control **(A** and **A')**, and *psme4* (1 ng) injected embryos **(B** and **B')**. RNA was injection into the vegetal pole at the 1-cell stage.

Table S1. An excel sheet to show proteomic analysis of proteasome components in the animal and vegetal hemisphere in 1-cell stage embryos.

Click here to Download Table S1

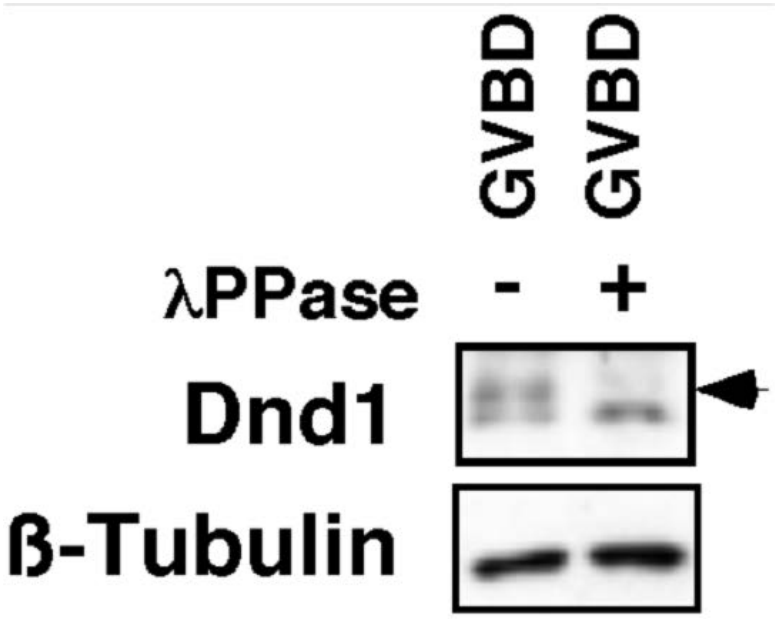

Figure S1. Phosphorylation of Dnd1 after oocyte maturation. (A) Western blot analysis showing the expression of endogenous Dnd1 in eggs (GVBD). Endogenous Dnd1 was enriched by IP from 50 eggs. Half of the IP sample was treated with λPPase. Arrow points to a band detected by anti-Dnd1 antibody, which migrates on SDS-PAGE relatively slowly. This band collapsed after phosphatase treatment, demonstrating that this is a phosphorylated form of Dnd1.

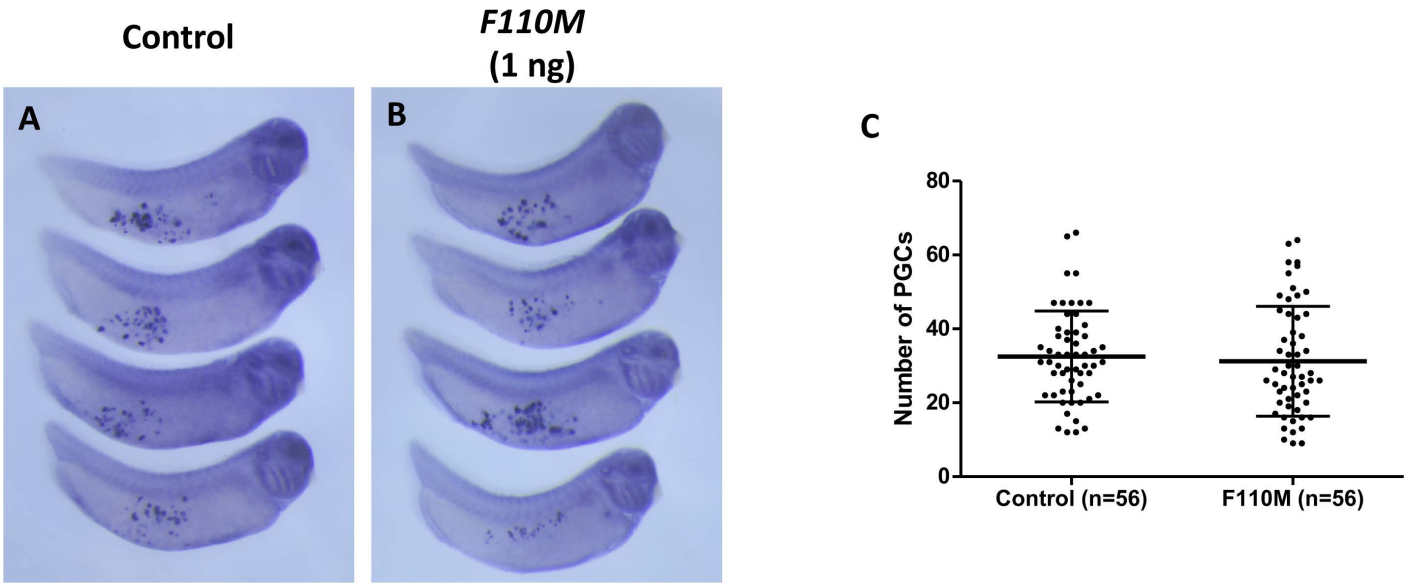

Figure S2. Overexpression of F110M had no effect on PGC development. (A) In situ hybridization showing the expression of *pgat* in control, and *F110M* (1 ng) injected embryos. RNA was injection into the vegetal pole at the 1-cell stage. **(B)** Quantification of results shown in **A**. The number of *pgat*-positive PGCs from each embryo was counted and plotted on the graph. There is no statistically significant difference between control and F110M overexpressed embryos.

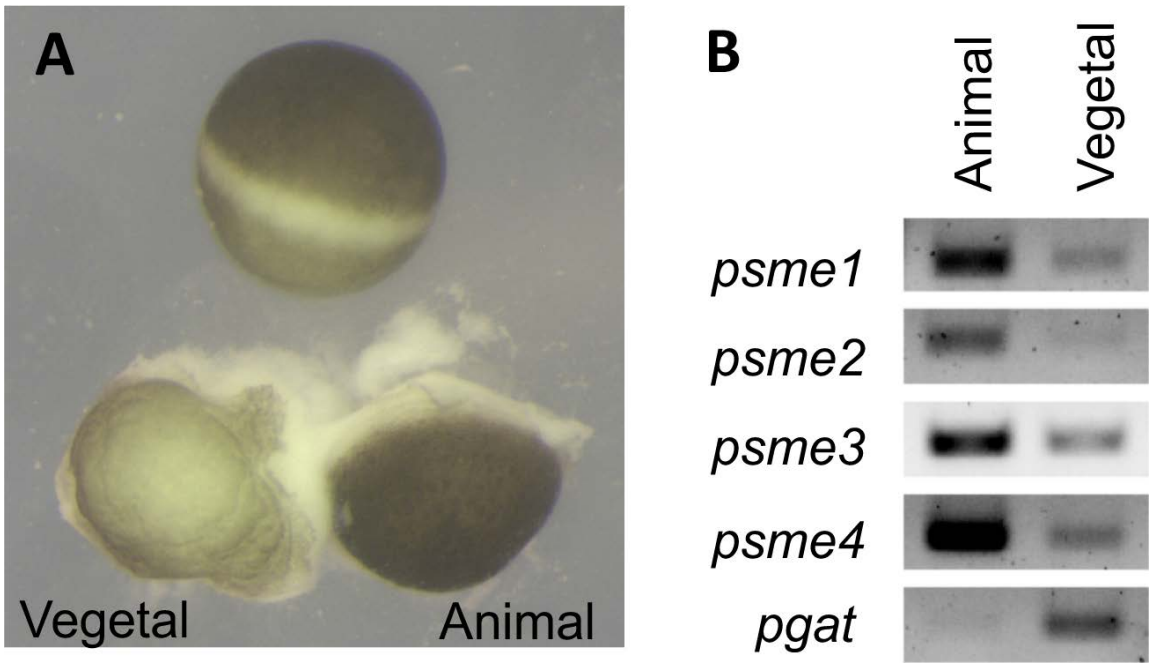

Figure S3. Asymmetric distribution of RNAs encoding ubiquitin-independent proteasome activator. (A) An intact stage VI oocyte and an oocyte that was dissected into animal and vegetal halves. **(B)** RT-PCR results showing the expression of *psme1*, *psme2*, *psme3*, *psme4*, and *pgat* in animal and vegetal halves of dissected oocytes. *pgat* was used as a marker for the vegetal hemisphere.

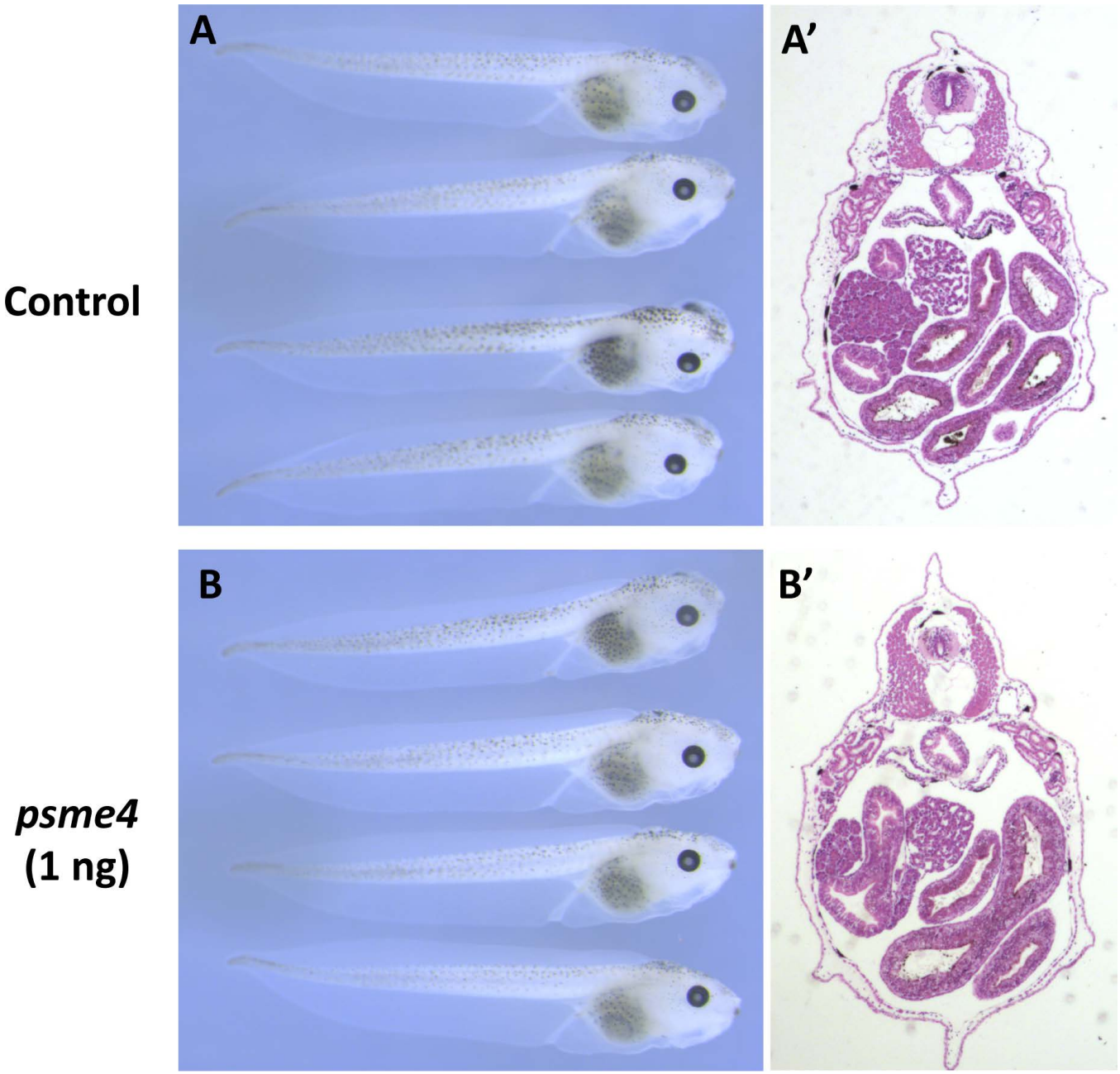

Figure S4. Overexpression of PSME4 had no effect on somatic development. Whole embryo morphology **(A** and **B)** and cross-section **(A'** and **B')** of control **(A** and **A')**, and *psme4* (1 ng) injected embryos **(B** and **B')**. RNA was injection into the vegetal pole at the 1-cell stage.

Table S1. An excel sheet to show proteomic analysis of proteasome components in the animal and vegetal hemisphere in 1-cell stage embryos.

Click here to Download Table S1